Cai *et al. Energy Mater.* **2025**, *5*, 500085
DOI: 10.20517/energymater.2024.266

Energy Materials

Review

Open Access

Advanced carbonaceous materials for Zn-ion hybrid supercapacitors: status and perspectives

Siyu Cai[1], Xinyan Zhou[2], Yi Wang[1,*], Xihong Lu[1,3,*]

[1]College of Chemistry and Material Engineering, Guiyang University, Guiyang 550005, Guizhou, China.
[2]Daqing Oilfield Design Institute Co., LTD, Daqing 163712, Heilongjiang, China.
[3]The Key Lab of Low-carbon Chem & Energy Conservation of Guangdong Province, MOE of the Key Laboratory of Bioinorganic and Synthetic Chemistry School of Chemistry, Sun Yat-Sen University, Guangzhou 510275, Guangdong, China.

[*]**Correspondence to:** Prof. Yi Wang, College of Chemistry and Material Engineering, Guiyang University, 103 Jianlongdong Road, Nanming District, Guiyang 550005, Guizhou, China. E-mail: wy742011@hotmail.com; Prof. Xihong Lu, The Key Lab of Low-carbon Chem & Energy Conservation of Guangdong Province, MOE of the Key Laboratory of Bioinorganic and Synthetic Chemistry School of Chemistry, Sun Yat-Sen University, 135 Xingang Xi Road, Haizhu District, Guangzhou 510275, Guangdong, China. E-mail: luxh6@mail.sysu.edu.cn

How to cite this article: Cai, S.; Zhou, X.; Wang, Y.; Lu, X. Advanced carbonaceous materials for Zn-ion hybrid supercapacitors: status and perspectives. *Energy Mater.* **2025**, *5*, 500085. https://dx.doi.org/10.20517/energymater.2024.266

Received: 29 Nov 2024 **First Decision:** 18 Dec 2024 **Revised:** 31 Dec 2024 **Accepted:** 9 Jan 2025 **Published:** 21 Apr 2025

Academic Editor: Wei Tang **Copy Editor:** Ping Zhang **Production Editor:** Ping Zhang

Abstract

Emerging Zinc-ion hybrid supercapacitors (ZHSCs) are being vigorously pursued due to their sustainability, economic efficiency, high safety and excellent theoretical electrochemical properties. As a significant element in the advancement of ZHSCs, carbonaceous materials can be utilized for fabricating the cathode and electrolyte and protecting the Zinc anode. Despite advancements, challenges notably persist in the form of unsatisfactory rate performance, scarcity of active sites, and undesirable cycling stability within carbonaceous cathodes. Here, this mini-review thoroughly expounds on the recent progress of carbonaceous materials with different dimensions and the corresponding synthesis strategies. The complexity of the structure, morphology, and relevant properties of sophisticated carbonaceous materials employed in contemporary devices is discussed. Besides, we elaborate on the strategies for modifying these materials to achieve optimal characteristics. Finally, the assessment of the existing challenges and prospects for carbonaceous materials within ZHSCs is explored. We anticipate that the insights presented herein can pave the way for developing carbonaceous materials, heading toward future-generation energy storage devices.

Keywords: Energy storage, zinc-ion hybrid supercapacitors, carbonaceous materials, cathode, electrochemical property

INTRODUCTION

Considering the dwindling reserves of fossil fuels and the carbon dioxide emissions, sustainable energy, particularly renewable clean energy sources, is experiencing rapid development. Therefore, there is an immediate requirement for efficient energy storage solutions, including electrochemical energy-storage devices (ESDs), among others[1,2]. In recent years, various ESDs have been extensively investigated and implemented across various applications, including metal-air batteries[3-6], aqueous ion batteries[7-10], supercapacitors[11-13], and other devices[14-19]. However, challenges remain inherent in both battery and supercapacitor technologies. Batteries are renowned for their exceptional energy density but are plagued by limited cyclic stability due to irreversible redox processes. Conversely, supercapacitors are celebrated for their enhanced power density and extended cycle life but offer a comparatively lower energy density when matched against batteries[20-25]. The concept of hybrid supercapacitors (HSCs) has emerged to integrate the distinct benefits of batteries and supercapacitors into a unified ESD. In HSCs, electrodes characterized by high capacity for abundant redox reactions serve as the energy reservoir. In contrast, electrodes featuring swift ionic conductivity can act as the power reservoir. This integration aims to enhance both the power and energy density of the system, thereby bridging the advantages of traditional batteries and supercapacitors[26-29]. Notably, it is posited that a meticulously engineered configuration of HSCs could remedy the limitation of both the batteries and supercapacitors. By enhancing the characteristics of each, HSCs exhibit a balanced solution suitable for various industrial applications[30-35]. Initially, hybrid capacitors with univalent metal ions such as Li^+, Na^+ and K^+ were studied, but these were constrained by resource scarcity and safety concerns. Subsequently, it has been discovered that polyvalent metal ions, such as Zn^{2+} and Mg^{2+}, offer more stable thermodynamics and faster charge transfer kinetics compared to univalent metal ions. This advantage arises because they have the capacity to store multiple electrons although the dynamic diameters of multivalent ions are similar to those of univalent ions[30,36]. Among polyvalent metal ions, zinc stands out due to its plentiful resources, high theoretical capacity (823 mAh g^{-1}), low redox potential [-0.76 V *vs.* standard hydrogen electrode (SHE)], compatibility with aqueous solutions, high safety, and eco-friendliness[28]. Here, we briefly compare the physical and chemical properties of different metals (Li, Na, K, Mg, Zn) for a more intuitive grasp of Zinc-ion HSCs (ZHSCs) [Table 1].

In this context, ZHSCs emerge as promising ESDs for fulfilling industrial requirements that address industry needs, striking a balance between the energy-rich Zn-ion batteries and the power-intensive supercapacitors[23,37,38]. These devices demonstrate remarkable performance and possess favorable traits, such as cost efficiency and safe enhancement. While various configurations are available, ZHSCs mostly consist of a zinc anode, an applicable cathode, and electrolytes containing Zn^{2+} ions[39,40]. Considering the diversity of energy storage mechanisms, the pattern of electrode materials in ZHSCs can be categorized into capacitor-type and battery-type. For capacitor-type electrodes, the ions are adsorbed/desorbed on the electrode surface to achieve efficient energy storage. The ZHSCs capitalize on the rapid adsorption/desorption mechanism facilitated by cathode materials and the reversible deposition/stripping mechanism on the Zn anode surface to store energy (Figure 1, Equation 1). Certain studies suggest that during the charging phase, anions from the electrolyte will attach to the surface of the positive electrode and are subsequently released back into the electrolyte upon discharging (Equation 2)[41,42]. Conversely, other research identifies completely opposite adsorption/desorption behaviors of Zn^{2+} ions (Equation 3)[43,44]. In addition, the cathodes can facilitate rapid redox processes if they contain oxygen functional groups or are doped with heteroatoms, and can enhance the capacitance of ZHSCs by contributing extra pseudocapacitance (Equation 4).

$$Zn \rightleftharpoons Zn^{2+} + 2e^- \quad (1)$$

Table 1. Distinguishing physical and chemical characteristics exhibited by Li^+, Na^+, K^+, Mg^{2+}, and Zn^{2+} ions within hybrid-ion capacitors

	Li^+	Na^+	K^+	Mg^{2+}	Zn^{2+}
Relative atomic mass	6.94	6.94	9.10	24.31	65.38
E_0 (A/A^{n+}_{aq}) V *vs.* SHE	-3.04	-2.71	-2.93	-2.37	-0.76
Shannon's ionic radii [Å]	0.76	1.02	1.38	0.72	0.74
Stokes radii in H_2O [Å]	2.38	1.84	1.25	3.47	3.49
Gravimetric capacity (mAh g^{-1})	3861	1166	685	2205	823

SHE: standard hydrogen electrode.

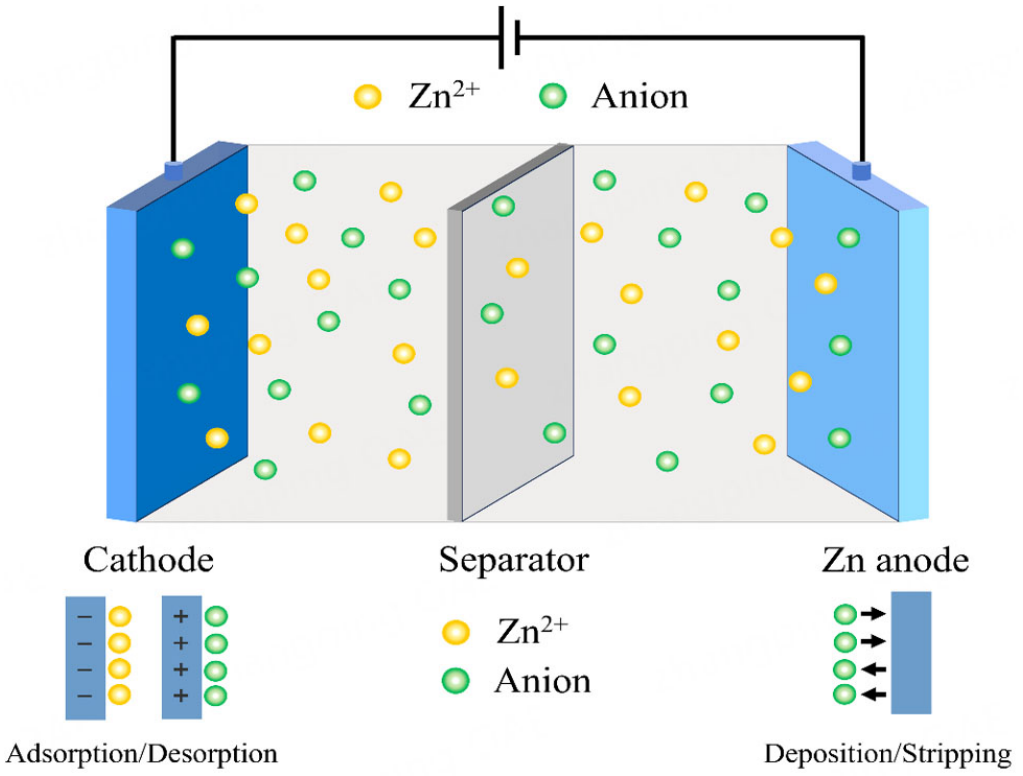

Figure 1. Schematic illustration of the charge storage mechanism in ZHSCs. ZHSCs: Zinc-ion hybrid supercapacitors.

$$\{C\} + X^- \rightleftharpoons \{C\}||X^- \quad (2)$$

$$\{C\} + Zn^{2+} \rightleftharpoons \{C\}||Zn^{2+} \quad (3)$$

$$\{C\}\cdots\cdots O + Zn^{2+} + 2e^- \rightleftharpoons \{C\}\cdots O\cdots Zn \quad (4)$$

Carbonaceous materials, including carbon materials and carbon-containing composites, possess adaptively adjustable pore structures, remarkable specific surface areas (SSA), swift transport rates of charge/ion, and outstanding structural stability [Figure 2]. These advantages make them ideal candidates for use as quintessential capacitive electrodes in ZHSC devices[45-47]. Electrodes fabricated by carbonaceous materials, boasting a large SSA, are capable of efficiently storing and releasing Zn^{2+} ions, thereby enhancing both the energy and power density of the ZHSCs[48]. The high SSA boosts ion conduction and consequently increases

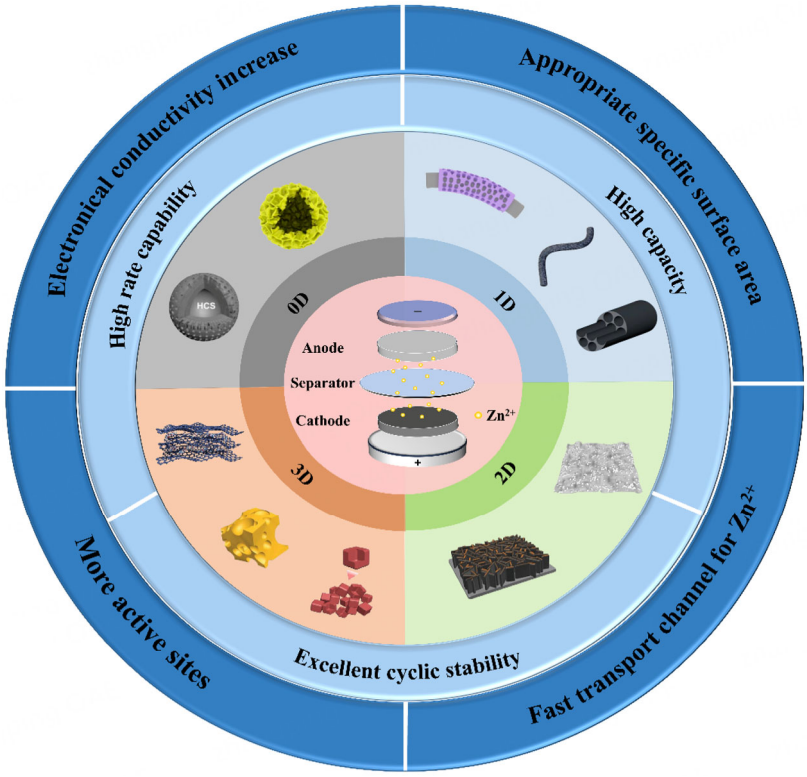

Figure 2. Diagrammatic representation of state-of-the-art carbonaceous materials for high-performance ZHSCs. ZHSCs: Zinc-ion hybrid supercapacitors.

energy/power densities of materials. The functions of porous carbonaceous materials in ion transport are contingent upon their pore size. The charge transfer resistance (Rct) is significantly influenced by micropores (less than 2 nm), mesopores (2 nm to 50 nm), and macropores (over 50 nm)[49]. An expanded surface area boosts the adsorptive capacity and increases porosity of a porous material. The porous nature of carbon-based electrodes ensures rapid electron and ion transport. Specially, Micropores are instrumental in the adsorption of ions onto the surface of electrode materials. Mesopores facilitate ion transfer by providing pathways for electrolyte ions. Meanwhile, macropores enhance ion transport, therefore reducing the diffusion resistance[50]. Additionally, carbonaceous materials with elevated electronic conductivity enable swift charge transfer and ion migration[51]. Furthermore, carbonaceous materials that exhibit exceptional mechanical strength and chemical inertness can preserve the structural integrity of electrodes throughout extensive cycling[52].

In 2016, Tian *et al.* pioneered the development of the original ZHSC, which features an oxidized carbon nanotube (oCNT) cathode paired with a zinc anode and a $ZnSO_4$ aqueous electrolyte[53]. Subsequently, extensive research on carbonaceous electrodes within ZHSCs has been inspired. For instance, Wang *et al.*[42] assembled ZHSCs employing activated carbon (AC) cathode, zinc anode, and zinc trifluoromethanesulfonate [$Zn(CF_3SO_3)_2$] in acetonitrile as the electrolyte. These ZHSCs demonstrated enhanced electrochemical performance and excellent durability. To date, a multitude of approaches have been put forth to enhance the performance of ZHSCs, yet several unresolved issues still exist in this field. These include the challenge of heterogeneous nucleation and side reactions at the zinc electrode[11,23], particularly the hydrogen evolution reaction (HER) to generate OH^- ions. These anions are capable of interacting with zinc ions (Zn^{2+}) in the aqueous electrolyte [such as $ZnSO_4$ and $Zn(CF_3SO_3)_2$], resulting in

the generation of insoluble compounds, as given in[54-56]

$$4Zn^{2+} + 6OH^{-1} + SO_4^{2-} + 5H_2O \rightleftharpoons Zn_4SO_4(OH)_6 \cdot 5H_2O \quad (5)$$

$$2Zn^{2+} + 4OH^{-1} + 2Zn(CF_3SO_3)_2 + 3H_2O_2 \rightleftharpoons [Zn(CF_3SO_3)_2Zn(OH)_2] \cdot 3H_2O \quad (6)$$

The formation/decomposition of $Zn_4SO_4(OH)_6 5H_2O/[Zn(CF_3SO_3)_2Zn(OH)_2]3H_2O$ on cathode electrodes is a reversible process that occurs during the charging and discharging. The researchers suggested that these side reactions might be responsible for a decrease in the capacity of ZHSCs. Conversely, other experts believe these reactions could contribute minimally to the whole energy storage[57]. As a result, there is a consensus that further in-depth study is required to fully understand the storage mechanism involved in these reactions. On the other hand, two main side reactions are involved at carbon cathodes: (1) carbon cathode may undergo oxidation at the surface, leading to the formation of oxygen-containing functional groups (such as carbonyl, carboxyl, or hydroxyl groups), which can modify the electrochemical behavior of the carbon cathode. In addition, carbon-active material will be lost due to excessive oxidation via CO_2 evolution; (2) Zn^{2+} released from the anode can migrate to the surface of carbon cathode during discharge, where they may react with hydroxide ions (OH^-) from the electrolyte (especially in basic or high-pH environments) to form zinc hydroxide [$Zn(OH)_2$]. The formation of this precipitate can block active sites on the carbon cathode and hinder the movement of charge carriers, which decreases the capacitance and stability of the carbon cathode.

In particular, the reported energy densities of ZHSC devices are significantly lower than theoretical values, and this diminished capacity for energy storage is largely due to the restricted ion adsorption occurring at the cathodes[30]. Thus, reasonable modifications to the carbon-positive electrodes have garnered increasing research interest. Previous research suggested numerous strategies to strengthen the adsorptive performance of carbon electrodes, including morphological adjustments, the construction of hierarchical porous structures, heteroatom doping into the carbon host, and oxygenic groups. For example, Huang *et al.*[58] indicated an anomalous increase in area-specific capacitance with a reduction in average pore size to below 1 nm. They also found that specific capacitance reached its maximum when the ionic size matched the pore dimensions of carbonaceous materials. Subsequent theoretical explorations demonstrated that desolvation effects arise as electrolyte ions infiltrate micropores[59]. Evidently, this phenomenon leads to a decrease in the radius of the electric double layer (EDL), thereby promoting an increase in specific capacitance under static electricity action. However, despite these promising advancements, the current capabilities of new carbonaceous materials have not yet met the high theoretical capacity of zinc electrodes, leading to somewhat unsatisfactory performance in ZHSC devices. It is crucial to further explore and refine the compatibility between SSA and dimensions of the pores within materials to fully understand the impact of electrolyte ions within pore structures. Moreover, achieving precise control over both pore size and structure-especially regarding micropores-remains a significant challenge. Over the past years, some researchers have devoted themselves to reviewing the synthesis processes and electrochemical properties of well-designed carbonaceous electrodes and the configurations of ZHSCs[60,61]. However, a comprehensive review including the latest design theories of carbonaceous electrode configurations and energy storage mechanisms is still needed, which can be instructional for future investigations of ZHSCs.

This review presents the mutual effect among structural engineering, pore characteristics, and energy storage mechanisms in carbonaceous electrodes. Here, we provide a comprehensive overview of the latest developments concerning sophisticated carbonaceous materials for ZHSCs, including design and fabrication strategy, structural configuration, and relevant properties. Subsequently, we outline modification

strategies to refine the electrochemical properties of the ZHSCs. Ultimately, the prevailing problems and potential opportunities for carbonaceous materials in ZHSCs are discussed, with the intention of fostering innovation in optimizing carbonaceous cathodes and therefore facilitating the advancement of ZHSCs with desired energy density.

ZERO-DIMENSIONAL CARBONACEOUS MATERIALS

Zero-dimensional (0D) carbonaceous nanomaterials are defined as matters that are nanoscale across all spatial dimensions, with sizes ranging from 1 nm to 100 nm[62]. Accordingly, the carbonaceous materials possessing 0D morphology specifically denote carbon nanoparticles. These new materials exhibit accelerated mass transfer rates due to their diminutive nanoscale dimension, distinctive nanostructure, and adjustable spherical size distribution. Among them, carbon spheres (CSs), carbon dots (CDs) and spherical carbon superstructures have emerged as the most extensively studied 0D carbonaceous materials within ZHSCs.

Hollow carbon spheres

Uniformly sized CSs possess several distinct advantages including superior electrical conductivity, regulable morphology of pores, and a size distribution that can be precisely controlled[63-65]. Thus, they demonstrate significant practicability to be employed for electrode materials in ZHSC applications.

Based on the structural features, the classification of CSs commonly includes several types, such as hollow CSs (HCSs)[66,67], yolk-shell structured CSs[68,69], and core-shell structured CSs[70,71], among others. These nanospheres were predominantly utilized in the fabrication of cathodes for ZHSC devices due to their nanostructure featuring large void space and high surface area. This unique structure facilitates mass transfer by promoting electrolyte ion diffusion while mitigating volume expansion during repeated charge-discharge cycles. Recent studies indicate that the performance of HCSs is significantly enhanced when nanostructures with interconnected open mesoporous channels, and precisely controlled shell thicknesses and channel lengths, are achieved[72]. Unfortunately, the majority of HCSs exhibit monotonous pore architectures, which constrains their effective utilization. The storage and transmission of Zn^{2+} ions within the micropores can be promoted by integrating a double-layer carbon shell with both micropores and mesopores[73]. It follows that the regulation and design of CSs with mesoporous hollow structures are of significant importance.

A synthesis strategy known as the hard template method is widely used to prepare HCSs. Specifically, a rational carbon precursor is selected to coat onto oxide spheres, which is subsequently converted into carbon through calcination, followed by the removal of the oxide template[74]. Resorcinol-formaldehyde (RF), Polyaniline (PANI) and Polydopamine (PDA) are representative carbon precursors reported in recent articles. Chen *et al.*[75] fabricated HCSs with mesoporous and defined these unique nanospheres as hollow mesoporous carbon spheres (HMCSs). The HMCSs originated from the core-shell structured SiO_2@RF nanoparticles, resulting in HMCSs with an appropriate SSA (800 $m^2 g^{-1}$). Then, they constructed a ZHSC using HMCSs to fabricate both the cathodes and functional coatings on the anode. The capacitance of obtained ZHSC attained 212.5 F g^{-1}. Meanwhile, an impressive retention of capacitance, with 99.4% maintained after 2,500 cycles, was achieved. Furthermore, RF resin had been regarded as a potential carbon precursor in the production of CSs. However, the practical applications of CS derived from phenol/formaldehyde resins remain limited due to the necessity of using highly carcinogenic phenol/formaldehyde and their failure to meet performance standards in certain domains. Du *et al.*[76] employed confined pyrolysis and leveraged polymerization characteristics of PDA to construct HCSs with a dual-shell structure comprising micropores and mesopores [Figure 3A-C]. The sizes of both micropores and mesopores could

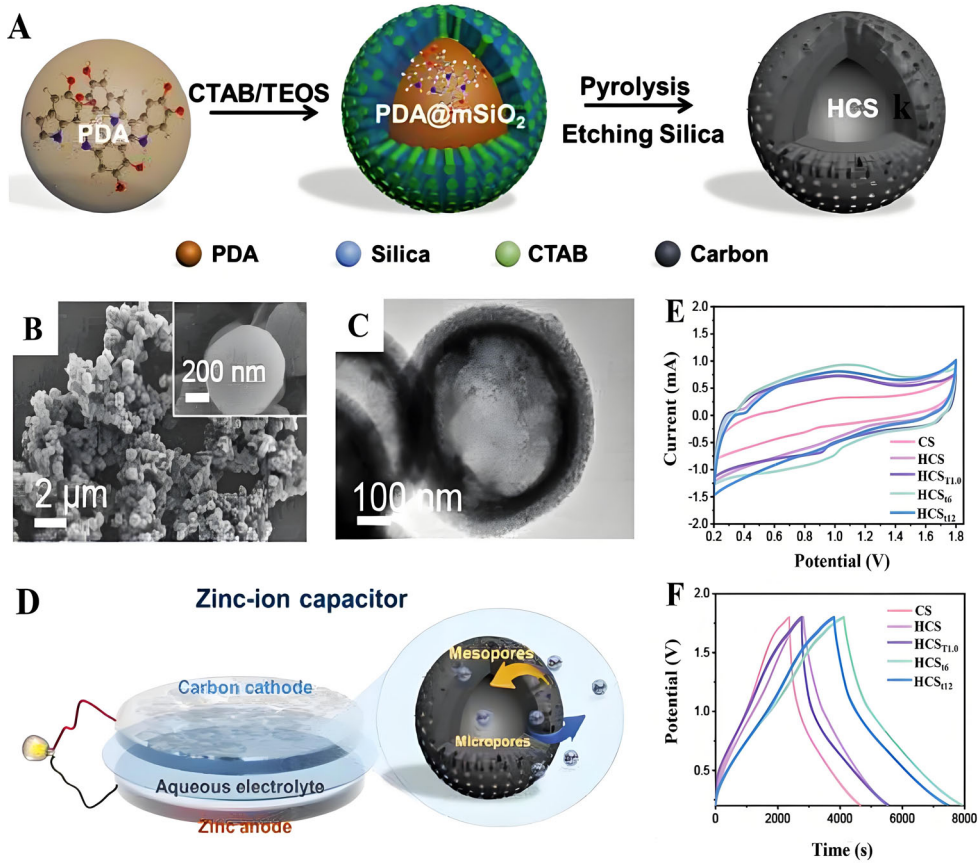

Figure 3. (A) Schematic of HCS synthesis; (B) SEM and (C) TEM images of HCSs; (D) Schematic diagram of ZHSC consisting of carbon cathodes and zinc anodes; (E) CV curves at a scan rate of 5 mV s^{-1}; (F) GCD curves at 0.1 A g^{-1}. Reproduced with permission from Ref.[76]. Copyright 2024, Wiley. HCSs: Hollow carbon spheres; SEM: scanning electron microscopy; TEM: transmission electron microscopy; ZHSCs: zinc-ion hybrid supercapacitors; CV: cyclic voltammetry; GCD: galvanostatic charge-discharge.

be delicately modulated by modifying the pyrolysis and hydrothermal synthesis processes. These regulable features of porosity link the depth of micro- and mesoporous in the resulting CSs to the specific capacity of ZHSCs. The cyclic voltammetry (CV) curves of the assembled ZHSCs (schematized in Figure 3D) displayed a broad operational voltage from 0.2-1.8 V [Figure 3E]. As illustrated in Figure 3F, the galvanostatic charge-discharge (GCD) curves exhibited discharge capacities of 147 F g^{-1} and 260 F g^{-1} at 0.1 A g^{-1} for CS and synthesized HCS, demonstrating that the capacitance of the ZHSCs could be enhanced when assembled by the cathode consisting of micropores/mesopores dual-shell carbon.

Besides, a MnO_2 hard template is employed to fabricate HCSs. For instance, a rational approach for the controlled synthesis of P/N dual-doped HCSs (PN-CHoNS) by introducing a flower-like MnO_2 template was proposed by Li *et al.*[77] [Figure 4A-C]. The MnO_2 nanoflowers serve dual functions that act both as structure-directing agents and chemical oxidative seeds. The structural features of 3D PN-CHoNS, including porous structure, hollow interior and dual doping engineering electronic structure, contributed to improved ion/electron transfer, enhanced contact between the electrolyte and electrode, and reduced path for ionic transport. Furthermore, the energy storage mechanism of PN-CHoNS was elucidated through the analysis of *in-situ* Raman spectroscopy. The results indicated the complementary benefits of electric double-layer capacitance (EDLC) and pseudocapacitance, which were respectively introduced by adsorption/desorption behaviors of physical and chemical ions, were significantly beneficial to improving

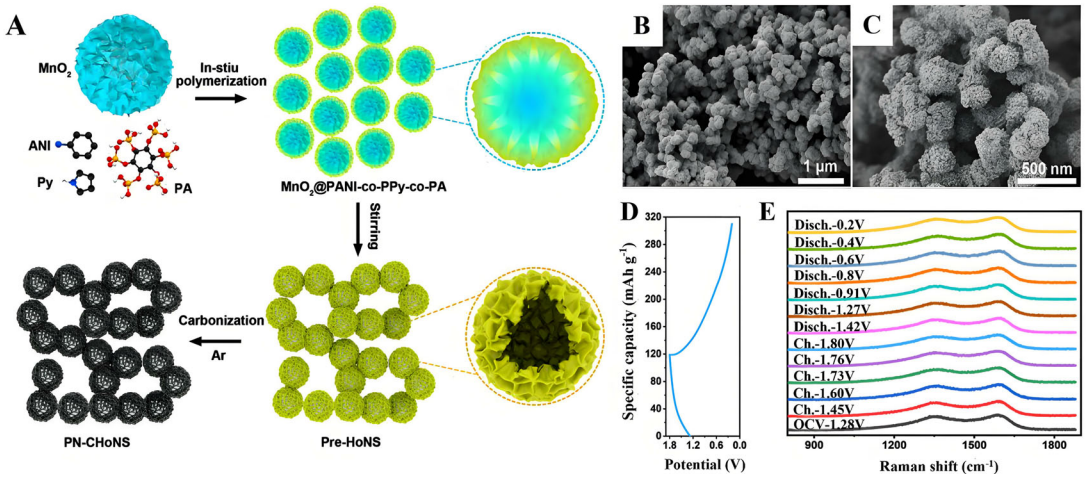

Figure 4. (A) Schematic diagram of the PN-CHoNS synthesis; (B and C) the SEM images of PN-CHoNS HSCs; (D) The charge-discharge profiles of ZHSC; (E) *In-situ* Raman spectra of PN-CHoNS cathode during charging/discharging process. Reproduced with permission from Ref.[77]. Copyright 2024, Elsevier. HSCs: Hybrid supercapacitors; PN-CHoNS: P/N dual-doped hollow carbon spheres; SEM: scanning electron microscopy; ZHSC: Zinc-ion hybrid supercapacitors.

the capacity of PN-CHoNS [Figure 4D and E]. The calculated results of density functional theory (DFT) evidenced that dual P and N doping enhanced the kinetics associated with the kinetics of absorption and desorption involving zinc ions. Thus, the prepared ZHSC device achieves excellent energy storage capacity (164.4 mAh g^{-1}). The calculated result of energy density was 116.0 Wh kg^{-1} at 141 W kg^{-1}, and remarkable cycling stability retaining 80.6% after 12,000 cycles was achieved.

Other 0D architectures

While HCSs demonstrate superior electrochemical properties, the thickness of the electrode can swell substantially under high mass loading, which consequently impairs electron conduction and ion diffusion, thereby diminishing the transport and storage capacity for Zn^{2+} ions. To tackle this issue, Liu *et al.*[78] introduced a spherical superstructure of CS_{30}, crafted through a Lewis pair interaction-guided self-assembly approach, to markedly improve the kinetics and Zn^{2+} storage of ZHSCs. The refined CS_{30} featured a gradient carbon framework containing lamellae and pores, which expedited ion migration and electron transfer, and enhanced Zn^{2+} storage. Throughout a 10-cycle duration, ZHSCs equipped with CS_{30} electrodes displayed superior rate performance, retaining a high capacity of 51.7% at 50 A g^{-1}, outperforming other counterparts with retention rates ranging from 7.2%-46.5%. Furthermore, elevating the mass loading of the active substances to 40 mg cm^{-2} resulted in ZHSC exhibiting a remarkable specific capacity of 132 mAh g^{-1}. Comprehensive research indicates that CS_{30} possesses a plethora of electrochemically active sites and swift mass transfer pathways, endowing it with rapid kinetics and superior zinc ion storage. Moreover, carbon nanodots have emerged as a candidate for electrode fabrication in ZHSCs, offering a mechanical buffer for the nanoparticle structure and facilitating rapid charge transfer. Guo *et al.*[79] synthesized a composite of carbon nanodots with Ni-Zn phosphates (CDs/NZP) through a straightforward hydrothermal process. By fine-tuning the concentration of CDs in the reaction, the chemical performance of the resulting hybrid structure was significantly enhanced. The combination of bimetal phosphates and the incorporation of CDs substantially improved the structural stability and electrical conductivity, which in turn expedited the charge transfer process, even under high current densities. When utilized as a pseudocapacitive electrode, this nanohybrid demonstrated an impressive specific capacitance of 1,885.7 F g^{-1} at a current density of 1 A g^{-1}, with a retention rate of 98.7% after 3,000 cycles. The outstanding performance of CDs/NZP was primarily attributed to the elaborated nanoparticle structure, the synergistic effect of the bimetal

phosphates, and the ultrafine CDs with high conductivity.

The pore morphology and structure of 0D carbonaceous materials is crucial for achieving superior electrochemical performance, yet the interplay between porosity and electrochemical behavior remains not fully understood. Xiao *et al.*[80] synthesized nitrogen-doped carbon with three distinct porous structures to investigate how size distribution of pores influences the electrochemical performance of ZHSCs, as depicted in Figure 5A. These porous carbon materials exhibit comparable specific surface area but different pore size distributions, which are defined to LVCR, LNCR and HVCR. The LNCR and HVCR are represent carbon materials lacking mesopores and macropores, respectively, whereas LVCR with hierarchical micro-, meso- and macropores. The optimized porous carbon (PC), referred to as LVCR, exhibited substantial electrochemically active surface area, an abundance of oxygen functional groups, and a hierarchical porous structure that enhanced electron transfer and ion diffusion [Figure 5B and C]. This hierarchical porosity, along with the presence of nitrogen doping, was instrumental in boosting the electrochemical performance of LVCR by facilitating efficient charge transport and maximizing the utilization of the active surface area. According to the results of *ex situ* characterizations [Figure 5D-G], the kinetics of Zn^{2+} storage were controlled by both macro- and mesoporous structures. The macroporous facilitated the transport of ions, while the mesoporous primarily boosted the capacity for Zn^{2+} storage. The outstanding electrochemical performance of LVCR could be credited to the swift, reversible processes of ion absorption and desorption, which were enabled by the hierarchical porous architecture. Consequently, the LVCR-based device exhibited an outstanding energy density of 126.6 Wh kg^{-1} at a power density of 31.4 kW kg^{-1}. Moreover, the device demonstrated exceptional stability, retaining a capacitance of 97.7% even after undergoing 50,000 cycles.

Obviously, 0D carbonaceous materials have exhibited great potential to be applied in electrode materials within ZHSCs. However, the structure control of these materials related to the characteristics of precursors is still an issue, especially for HCSs. Previous works have indicated that the thickness can only be increased by introducing a precursor layer and coating it layer by layer, while the pore size distribution is limited by mesopores[81]. This is not only time-consuming but also hinders macro preparation of 0D carbon materials. Therefore, further optimization of the synthetic route to fabricate elaborate nanostructure with adjustable dimensions and hierarchical pore size distributions is significant and urgently needed.

ONE-DIMENSIONAL CARBONACEOUS MATERIALS

Carbonaceous materials characterized by one-dimensional (1D) nanostructures are increasingly recognized as viable options for electrode materials in ZHSCs[82,83]. These materials are distinguished by their high aspect ratio, which contributes to their superior electronic conductivity, and their remarkable mechanical flexibility. The synergistic effect of these attributes allows for facilitating efficient electron transfer if the 1D carbonaceous materials were used to construct cathode in ZHSCs. Additionally, the exceptional mechanical stabilities of 1D carbonaceous materials render them highly suitable for the advancement of flexible or wearable electronic devices, presenting a clear advantage over traditional planar structures[84,85]. The carbon nanotubes (CNTs) and carbon nanofibers (CNFs) are particularly notable for their exemplary performance.

Carbon Nanotubes

CNTs are regarded as descendants of fibrous carbon materials and fullerenes[85]. Owing to their remarkable chemical and mechanical properties, including high tensile strength, ultra-lightness, unique open pore structure, and high chemical stability[86], CNTs are recognized as promising electrode materials. Based on the CNTs, Zhang *et al.*[87] presented a Zn-ion hybrid fibrous supercapacitor (ZnFC), which was assembled by a cathode fabricated by a fibrous material composed of reduced graphene oxide (rGO) and CNTs. This

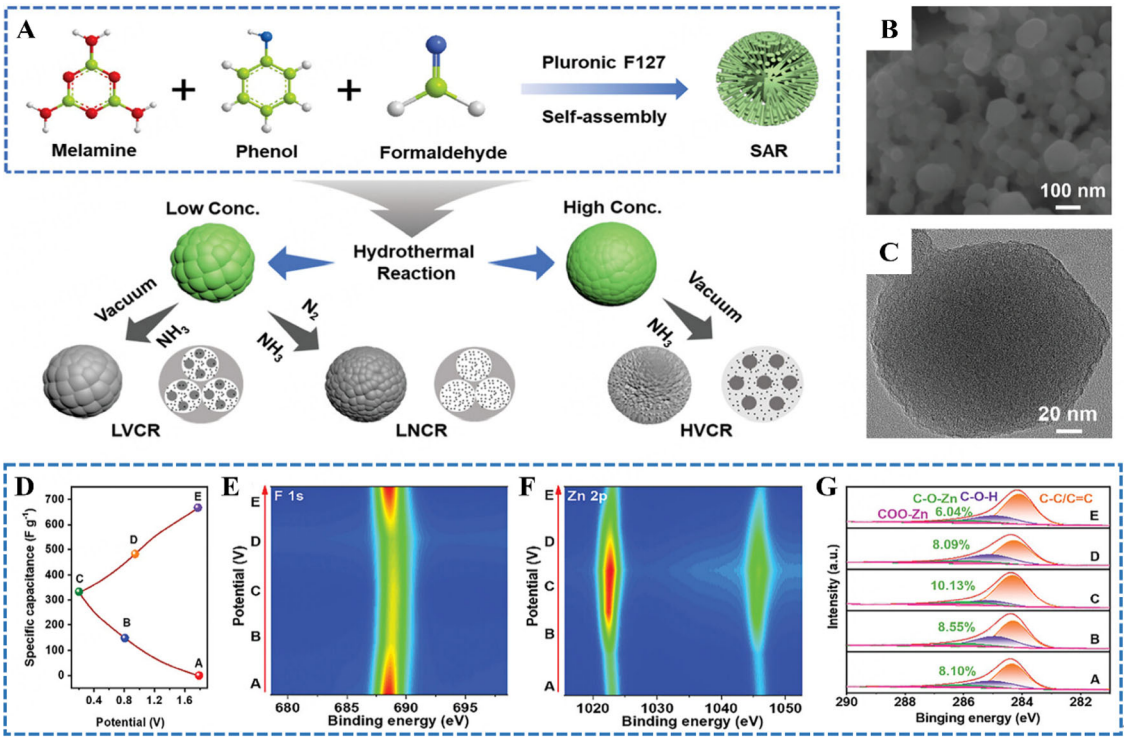

Figure 5. (A) Schematic illustration for the synthesis of LVCR, LNCR and HVCR; (B) SEM and (C) TEM images of LVCR; (D) GCD curves of LVCR with selected points assigned to different charge/discharge states; 2D contour images of (E) F 1s Zn 2p and (F) Zn 2p; and (G) high-resolution XPS spectra of C 1s. Reproduced with permission from Ref.[80]. Copyright 2024, Wiley. SEM: Scanning electron microscopy; TEM: transmission electron microscopy; GCD: galvanostatic charge-discharge; 2D: two-dimensional; LVCR: hierarchical micro-, meso-and macropores; LNCR: carbon materials lacking mesopores; HVCR: carbon materials macropores.

supercapacitor exhibited an excellent specific capacitance (104.5 F cm^{-3} at 0.4 A cm^{-3}) owing to its capacitor-type cathode. Subsequently, Lin *et al.*[88] developed a ribbon-shaped composite containing multi-walled CNTs and graphene oxide. This composite, named Nanoporous multi-wall carbon nanotube@graphene oxide nanoribbons (NP-MWCNT@GONR), was synthesized by $ZnCl_2$ activation to form core-shell structure with a SSA of 54.2 m^2 g^{-1}. The chemical properties and stabilities of ZHSCs with the NP-MWCNT@GONR were significantly higher than that with blank materials synthesized without activation, involving a specific capacitance of 185.3 F g^{-1} at 0.1 A g^{-1} and an energy density of 90.09 Wh kg^{-1} at 95 W kg^{-1}.

However, compared with other carbonaceous materials, the relatively low SSA and density of the CNTs restrict the enhancement of capacitance and energy density[89]. Thus, it is urgently necessary to increase the amount of pseudocapacitive active sites in CNTs. Recent studies are devoted to modifying CNTs by doping with heteroatom (e.g., N, O, P) to improve the pseudocapacitive active sites. Yang *et al.*[90] synthesized a flexible CNT@PC foam by carbonizing the phenol-modified micelles from melamine with Pluronic F-127 *in-situ* onto CNTs [Figure 6A and B]. Through the carbonization of precursors, the co-doped nitrogen and oxygen with high concentration was accomplished. The slender PC films, measuring 12.5 nm in thickness [Figure 6C], could provide a brief path of ionic transport and were characterized by a substantial number of open mesopores. These unique mesopores have an average diameter of 14.3 nm and account for a significant 64.7% mesopore volume ratio. In the resultant ZHSC, an excellent specific capacity of 175.3 mAh g^{-1} at 0.1 A g^{-1}, a high energy density of 150.8 Wh kg^{-1} at 80 W kg^{-1} and an impressive rate capability of 93.1 mAh g^{-1} at 50 A g^{-1} were achieved. The examination of the electrochemical storage

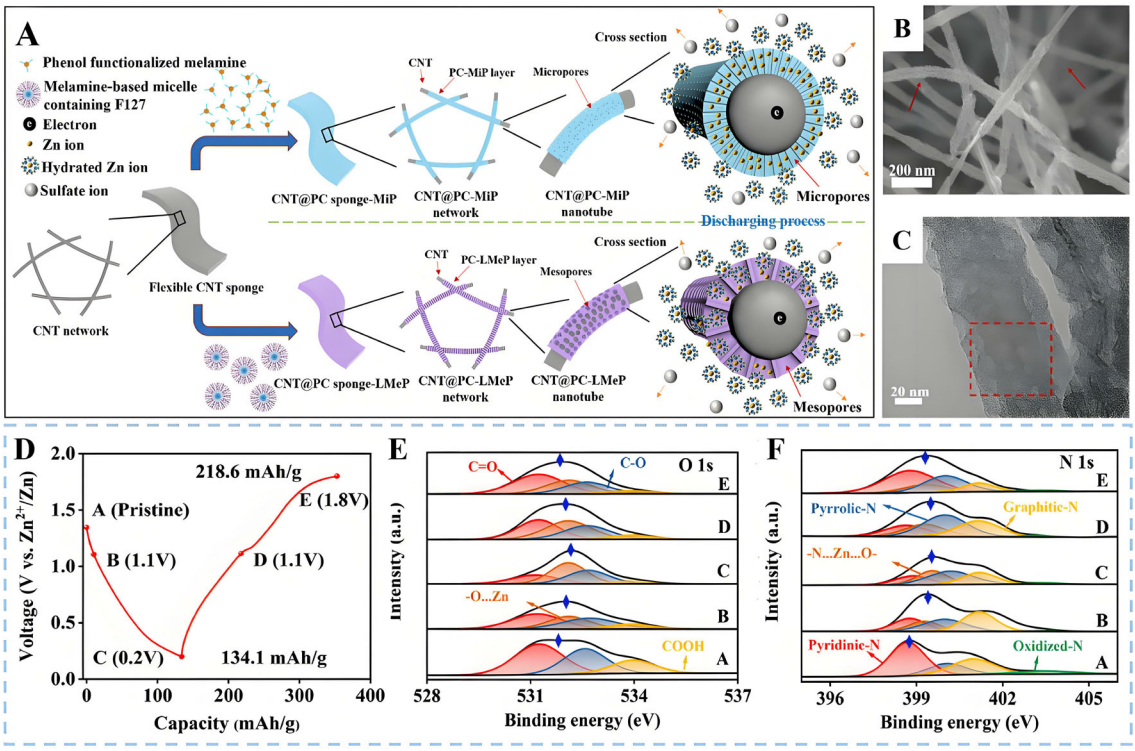

Figure 6. (A) Schematic of CNT@PC synthesis; (B) SEM and (C) TEM images of CNT@PC foam; (D) The first GCD curve of CNT@PC foam at 0.1 A/g; *Ex-situ* (E) O 1s and (F) N 1s XPS spectra of CNT@PC foam. Reproduced with permission from Ref.[90]. Copyright 2024, Elsevier. SEM: Scanning electron microscopy; TEM: transmission electron microscopy; GCD: galvanostatic charge-discharge; XPS: X-ray photoelectron spectroscopy; CNT: carbon nanotube; PC: porous carbon.

mechanisms of the CNT@PC cathode was conducted using *ex-situ* X-ray photoelectron spectroscopy (XPS) analysis at five specific stages, as illustrated in Figure 6D-F. During the initial discharge process, the *ex-situ* O 1s spectra demonstrated a progressive shift towards higher energy in the peak's location [Figure 6E]. This shift signified a decrease in the peak's intensity at 531.3 eV, associated with the carbonyl group, and the appearance of a peak at 532.1 eV, corresponding to the C-O-Zn bond. The formation of new Zn-containing bonds suggested that Zn ions were being adsorbed onto the CNT@PC cathode throughout the discharge process. The shift of N 1s spectra also indicated a reversible process of Zn ion desorption from the CNT@PC foam cathode [Figure 6F]. Electrochemical kinetic analyses also showed that the utilization of CNT@PC foam significantly increased capacitive contributions (73.6%), while the diffusion resistance was reduced to 23.6 Ω/s1/2. Notably, the multilayer CNT@PC sponge exhibited a nearly linear rise in areal capacity as the number of layers grew. Compared with the energy densities reported for ZHSCs[91-95], the 5L-stacked CNT@PC foam cathode displayed higher energy density of 0.29 mWh cm^{-2} at 1.6 mW cm^{-2} and power density of 0.12 mWh cm^{-2} at 32 mW cm^{-2}, respectively.

CNFs

In recent times, there has been extensive exploration of CNFs as prominent carbonaceous materials for ZHSCs. The remarkable characteristics of CNFs, such as affordability, superior electrical conductivity, excellent flexibility, remarkable thermal stability, and lightweight nature, greatly improve their charge storage performance[96]. The electrospinning method, as a versatile technique to produce CNF connective framework, can extend surface areas, nanoscale diameters, flexibility, porosity, and high interconnectivity of CNFs[97]. Moreover, it is possible to boost the electronic conductivity and hydrophilicity of CNFs by modifying their surface, while also enhancing the chemisorption of ions. He *et al.*[98] devised a flexible CNF

film featuring oxygen-containing groups using a simple method. These oxygen-containing groups significantly enhanced the wettability of the carbon fibers with aqueous electrolytes and greatly promoted the chemical absorption of Zn^{2+} ions to improve the capacitance. The ZHSC assembled with a cathode made of this carbon fiber achieved remarkable energy and power densities. Li *et al.*[99] created specific carbon fibers characterized by a hierarchical porous architecture and functional groups containing heteroatoms of oxygen and nitrogen. The capacitance of assembled ZHSC attained 156 mAh g^{-1}, and high energy and power densities of 127 Wh kg^{-1} and 15.3 kW kg^{-1} were obtained, respectively. Investigations into the mechanisms revealed that the charging/discharging cycles of the CNF cathodes involved the adsorption and desorption of cations, along with the formation and dissolution of $Zn_4SO_4(OH)_6 \cdot 5H_2O$ at lower voltages, whereas anion adsorption and desorption occurred at higher voltages.

In practical applications, synthetic materials must be coated onto a current collector to form cathodes[100]. Nevertheless, these current collectors commonly exhibit restricted SSA and insufficient active adsorption sites on their surface[101,102], which hampers the energy density enhancement of ZHSCs[103]. Thus, there is an urgent requirement to engineer sufficient active sites of the current collector and to employ them directly as flexible cathodes in ZHSCs. As illustrated in Figure 7A-C, He *et al.*[104] designed an *in-situ* exfoliation method to incorporate highly nitrogen-doped pyridine/pyrrole (Py) and carbonyl-functionalized nanosheets onto a CNF framework (N-OPCNF). The obtained N-OPCNF film featuring numerous active sites could be utilized as a self-supporting cathode for ZHSCs. Following the exfoliation of the nitrogen-doped pyridine/Py and carbonyl-modified nanosheets, the architecture of the CNFs underwent partial opening, facilitating the accumulation and diffusion of Zn^{2+} throughout the entire CNFs. The calculation results of DFT suggested a marked improvement of electrochemical activity stemming from a multitude of highly active chemisorption sites [Figure 7D]. Utilizing this method, the capacitance of the obtained cathode increased to 136 mAh g^{-1}. The researchers assembled a quasi-solid ZHSC using N-OPCNF cathode and gelatin electrolyte [Figure 7E]. The ionic conductivity (σ) of the gelatin electrolyte was calculated to be 3.67 ms cm^{-1} according to

$$\sigma = \frac{L}{AR} \tag{7}$$

where R represented the ohmic resistance, L indicated the thickness, and A denoted the area of the gel electrolyte. Notably, the series CV test results under simulated actual application conditions indicated that by connecting two devices, the combined capacitance could indeed be doubled [Figure 7F]. The obtained ZHSC possessed an extended cycle life, maintaining a capacitance retention rate of 80.38% following 8,000 cycles at 1 A g^{-1} [Figure 7G].

Introducing a heteroatom can further enhance the chemical properties of CNFs by generating many defects on the surface by modifying the type of hybrid orbitals in carbon atoms[105]. Moreover, modifications in the porosity can result in the loss of atoms and alterations to the distortion within the crystal lattice. These mechanisms can give rise to a multitude of intrinsic defects that are structurally induced, such as edge sites, vacancies, and pores[106]. Zhang *et al.*[107] proposed a new strategy for designing hollow CNFs that featured multi-channel and a graphene-analogous structure and a notably large SSA, named Multi-channel hollow carbon nanofiber (MCHCNF) [Figure 8A-C]. Through the strategy of pore construction and expansion, the dual objectives of increasing active site quantity and eliminating diffusion barriers are achieved simultaneously. Featuring a SSA of 2,511.1 m^2 g^{-1}, the optimized structure of MCHCNF exhibits highly developed hierarchical pores. The DFT results, as shown in Figure 8D, confirmed the significant reduction of the energy threshold for reactions between the defect and active ions, consequently boosting the chemisorption of ions. Importantly, the MCHCNF is characterized by an appropriate micropore size

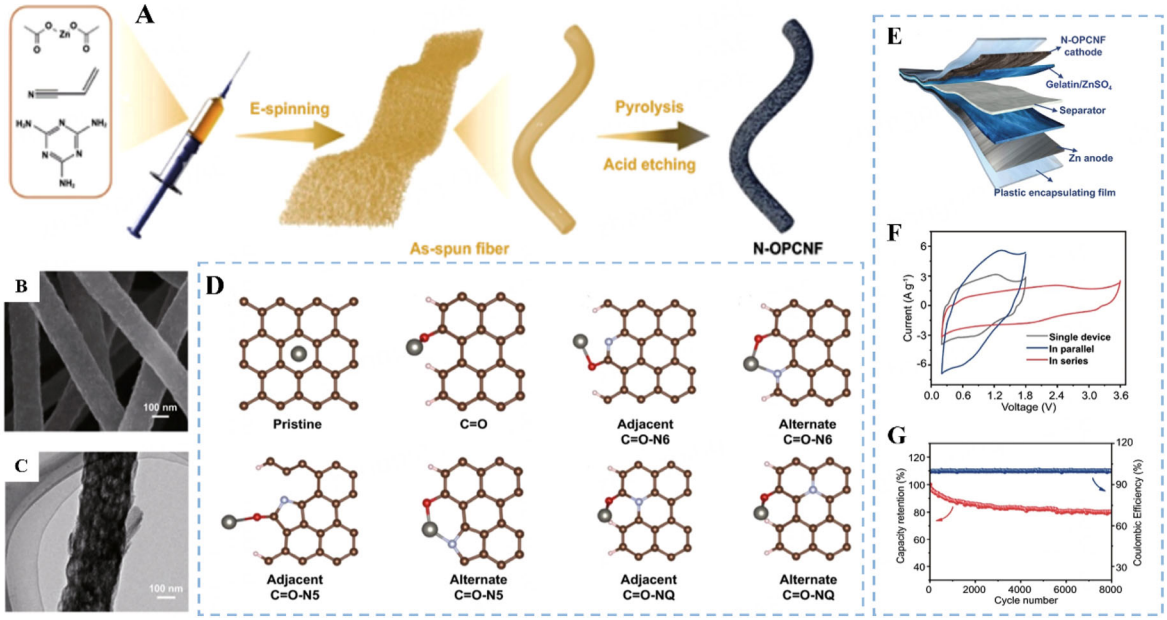

Figure 7. (A) Schematic of N-OPCNF synthesis; (B) SEM image and (C) TEM image; (D) The results of theoretical calculations for the Zn adsorption; (E) Schematic diagram of the assembly of ZHSC; (F) CV profiles; (G) Capacitance retention and coulombic efficiency. Reproduced with permission from Ref.[104]. Copyright 2024, Springer. N-OPCNF: Nanosheets onto a arbon nanofiber framework; SEM: Scanning electron microscopy; TEM: transmission electron microscopy; ZHSC: Zinc-ion hybrid supercapacitor; CV: cyclic voltammetry.

between 0.86 nm and 2 nm and well-developed mesopores, which significantly boost the embedding of $[Zn(H_2O)_6]^{2+}$/hydrated CF_3SO^{3-}. Consequently, it provided a remarkable specific capacity attaining 191.4 mAh g^{-1}, and reasonable capacitance retention of 93.0% across 15,000 cyclic processes. Calculated energy and power densities were as high as 133.1 Wh kg^{-1} and 34.4 kW kg^{-1}, respectively.

In conclusion, CNTs and CNFs demonstrate impressive conductivity, durable chemical stability, and the capability to facilitate a direct pathway for electron transfer. In contrast to two- (2D) and three-dimensional (3D) carbon forms, the limitation of 1D carbon lies in its lower capacitance resulting from restricted SSA and reduced packing density. Nowadays, investigations into CNTs have predominantly focused on integrating them with additional active components to establish improved conductive pathways within the cathodes. The doping of heteroatoms (e.g., N, P, S) can significantly improve the wettability of 1D carbonaceous materials and accelerate the transfer of Zn^{2+} ions. Furthermore, the employment of CNFs as current collectors is projected to optimize the functionality of ZHSCs.

2D CARBONACEOUS MATERIALS

In the development of electrode materials, 2D carbonaceous materials are particularly prominent. Owing to the elaborately engineered structures and modified electronic properties, 2D layered PCs show extraordinary potential in energy-related applications by fostering stronger interactions between components[108]. Their expanded interlayer spacing offers an expansive surface area and exposes a larger number of reactive atoms and electrochemically active sites to enhance the capacitance. This section concentrates on two widely investigated 2D carbonaceous materials: graphene-based materials and carbon nanosheets.

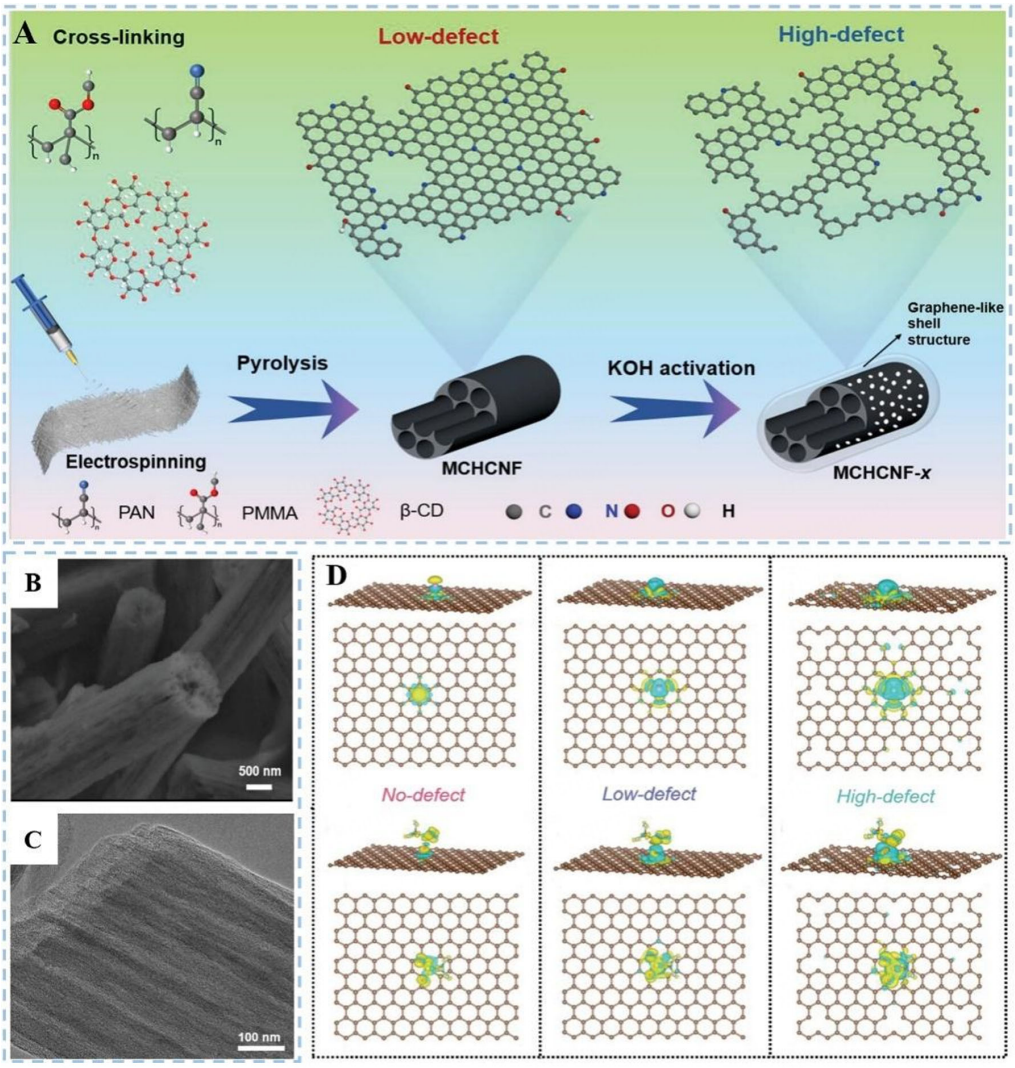

Figure 8. (A) Diagrammatic representation of the fabrication procedure of MCHCNF and MCHCNF-x (h); (B) Electron microscopy characterization and (C) TEM images of MCHCNF; (D) The results of DFT of Zn^{2+}/ CF_3SO^{3-} adsorption. Reproduced with[107]. Copyright 2023, Wiley. TEM: Transmission electron microscopy; DFT: density functional theory; MCHCNF: multi-channel hollow carbon nanofiber.

Graphene-based materials

As a representative 2D carbonaceous material, graphene is formed by carbon atoms arranged in a hexagonal lattice through sp^2 hybridization[89]. Its unique properties, including a definite pore structure, remarkable inertness, exceptional electrical conductivity, and an extraordinarily high theoretical SSA-reaching up to 2,630 m^2 g^{-1}-render graphene enormous potential for being applied as a cathode material in various applications[23]. Research conducted by Wu *et al.*[109] was the first to illustrate the potential of graphene for fabricating cathodes eligible for use in ZHSCs. The researchers crafted a cathode by utilizing a modified Hummers' method to produce porous carbon derived from chemical activated graphene (aMEGO), which was subsequently activated with KOH. The setup resulted in the construction of a Zn//aMEGO ZHSC, also encompassing a zinc anode with an electrolyte solution of 3M $Zn(CF_3SO_3)_2$. This device exhibited impressive cycling stability that retained 93% capacitance after an astonishing 80,000 cycles at 8 A g^{-1}, indicating a durability level comparable to traditional electric double-layer capacitors. In another noteworthy contribution, Sun *et al.*[110] presented a hybrid device that effectively combined features of both

pseudocapacitive materials and Zn-air batteries within a ZHSC framework. The achievement was made possible by employing a rGO foam (RG-R). This PC material contained abundant defects and oxygen functional groups, improving the wettability of the pore surface and providing extra active sites. The performance of the Zn//RG-R ZHSC was assessed under two configurations: in ambient air and as a coin cell. The results indicated a significant improvement in discharge times in the air, where the device demonstrated a performance of 370.8 F g^{-1} at 0.1 A g^{-1}, contrasting with a lower performance of 200.4 F g^{-1} at 0.1 A g^{-1} when tested as a coin cell. This discrepancy suggested that the defects distributed in the graphene structure might serve as active sites conducive to catalyzing redox reactions, contributing to enhanced overall device performance.

Nevertheless, it was essential to recognize that the beneficial chemical performance of graphene-based materials could be hindered by the material's propensity to aggregate and restack, which posed challenges for their optimal functionality. To tackle this issue, Song *et al.*[111] created a graphene@carbon cloth (CC) cathode by means of coating the flexible CC with the colloids of graphene nanoflakes, which effectively reduces the aggregation and restack of graphene. The graphene@CC cathode exhibited a SSA of 678.6 m^2 g^{-1}, characterized by a significant presence of mesopores. A substantial specific capacitance of 247.7 F g^{-1} at 0.2 A g^{-1} and an energy density of 158.1 Wh kg^{-1} at 0.2369 kW kg^{-1} were achieved by assembling ZHSC utilizing graphene@CC cathode. In addition, this ZHSC demonstrated outstanding stability over extended cycling, retaining 73.7% of the initial capacitance after 50,000 cycles. Furthermore, even at low temperatures such as 20 °C, this device maintained a notable capacitance of 202.8 F g^{-1} at the same current density, equating to 81.9% of its original capacitance measured at ambient temperature.

The other effective strategies to prevent the aggregation and stack of graphene involve combining graphene-based materials with other nanomaterials. Notably, metal-organic framework (MOF)-derived carbonaceous materials are a potential method to expose maximum active sites and have been employed in new ESDs[112,113]. Jia *et al.*[114] synthesized a composite consisting of MIL-88B(V) nanorods integrated with rGO sheets [MIL-88B(V)@rGO] using a simple hydrothermal synthesis method. This approach effectively mitigated the aggregation and stacking of GO and regulated the crystallization of MIL-88B(V); thus, uniformly fine nanorods were obtained [Figure 9A-C]. Throughout the first charging/discharging cycle, the MIL-88B(V) underwent a conversion into amorphous V_2O_5 due to electrooxidation, promoting the insertion/ extraction behaviors of Zn^{2+} by offering the primary active sites. Moreover, the rGO sheets created uninterrupted electron transfer routes and avenues for ion diffusion, which expedited the redox reactions and enhanced the pseudocapacitive performance. As demonstrated in Figure 9D and E, the amorphous V_2O_5@rGO exhibited outstanding electronic conductivity, a negative Zn^{2+} adsorption energy of (-0.715 eV), and low energy requirements for Zn^{2+} insertion (0.814 eV) and extraction (0.332 eV). Therefore, the MIL-88B(V)@rGO delivered an impressive specific capacity of 479.6 mAh g^{-1} at a current density of 50 mA g^{-1}, alongside an improved cycling stability, retaining 80.3% of the initial capacity after 400 cycles at 2 A g^{-1}. It should be noticed that the assembled pouch cell featuring the prepared cathode and a Zn anode [Figure 9F], which were subjected to 90°, 120°, and 180° bends, demonstrated stable discharge capacities and voltages [Figure 9G and H]. The remarkable flexibility and stability of the MIL-88B(V)@rGO rendered it suitable for applications in flexible ZHSCs.

A straightforward self-adaptive method was recommended by Wu *et al.*[115], which involved simultaneous production of cathodic materials alongside anodic protective coatings. In Figure 10A, GO and acrylamide (AM) are employed to facilitate electro-polymerization of Py, resulting in the formation of doped polypyrrole (PPy) composites, denoted as PPy/GO-AM. These composites are specifically engineered for the construction of a capacitive-type cathode. Throughout this methodology, a self-assembled composite

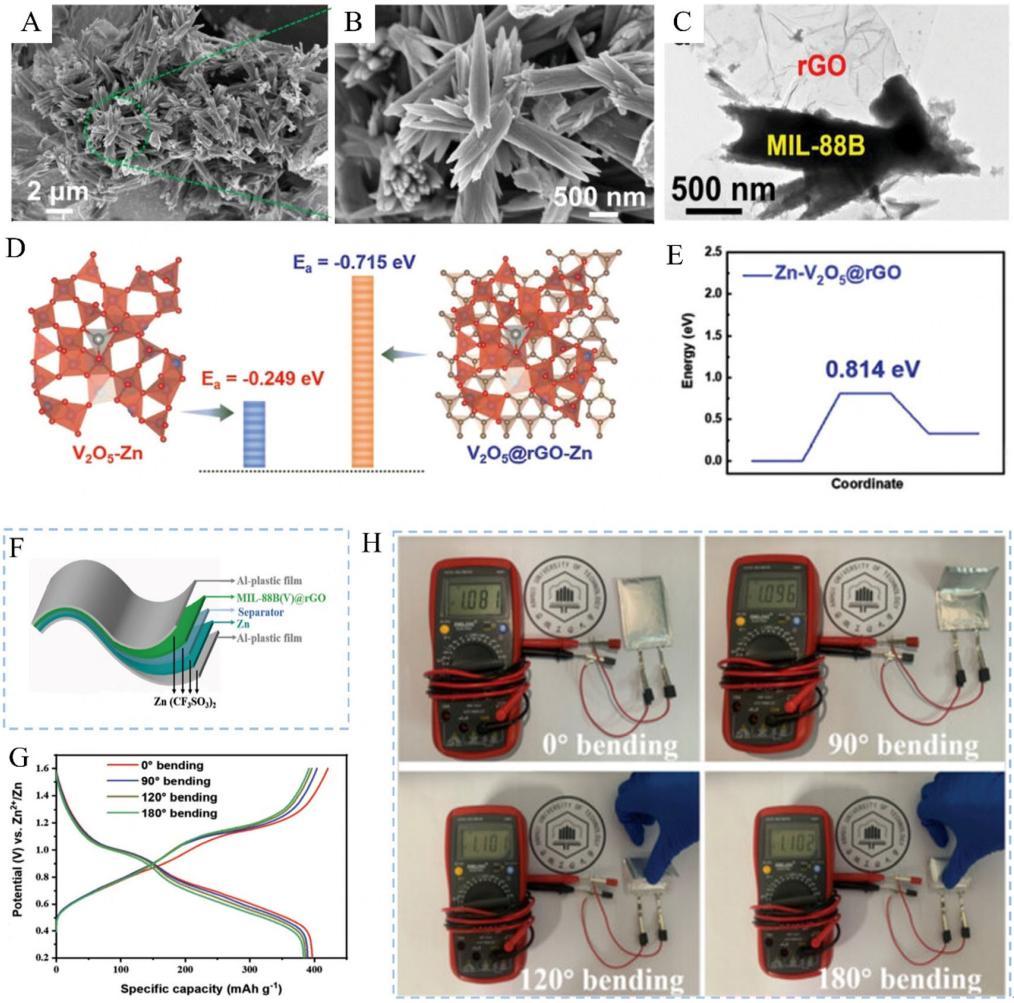

Figure 9. (A and B) SEM and (C) TEM images of MIL-88B(V)@rGO composite; (D) The calculated Zn^{2+} adsorption energy; (E) The calculated insertion/extraction energy of Zn^{2+} in amorphous V_2O_5@rGO; (F) Schematic diagram of a flexible pouch cell; (G) The GCD curves under different bending angles; (H) The voltage of samples bent to different angles. Reproduced with permission from Ref.[114]. Copyright 2024, Wiley. SEM: Scanning electron microscopy; TEM: transmission electron microscopy; GCD: galvanostatic charge-discharge; rGO: reduced graphene oxide.

layer made up of rGO and polyacrylamide (PAM) is deposited onto the Zn foil (rGO/PAM@Zn). The CV curves obtained at various scanning rates display distorted rectangular patterns [Figure 10B]. These curves suggested dual mechanisms of energy storage: the accumulation of electrolyte ions on the electrode surface through electrostatic adsorption, and the pseudocapacitance stemming from the insertion/extraction of ions within electrolyte. The ZHSC was assembled utilizing these two optimized electrodes [Figure 10C], which exhibited an ideal rate performance calculated from the GCD curves exhibiting an excellent specific capacitance of 125 mF cm^{-2} at 1 mA cm^{-2}, and an impressive specific capacitance of 125 F cm^{-3} at a current density of 1 mA cm^{-2} [Figure 10D]. The computed energy density reached 0.044 mWh cm^{-2} at a power density of 0.8 mW cm^{-2}. Additionally, a remarkable cycling stability of the ZHSC was also obtained, which evidenced a 90.3% retention after 5,000 cycles [Figure 10E]. The self-adaptive optimization strategy provided advantageous mechanical properties for flexible ZHSCs, making this manufacturing technique scalable and easily adaptable.

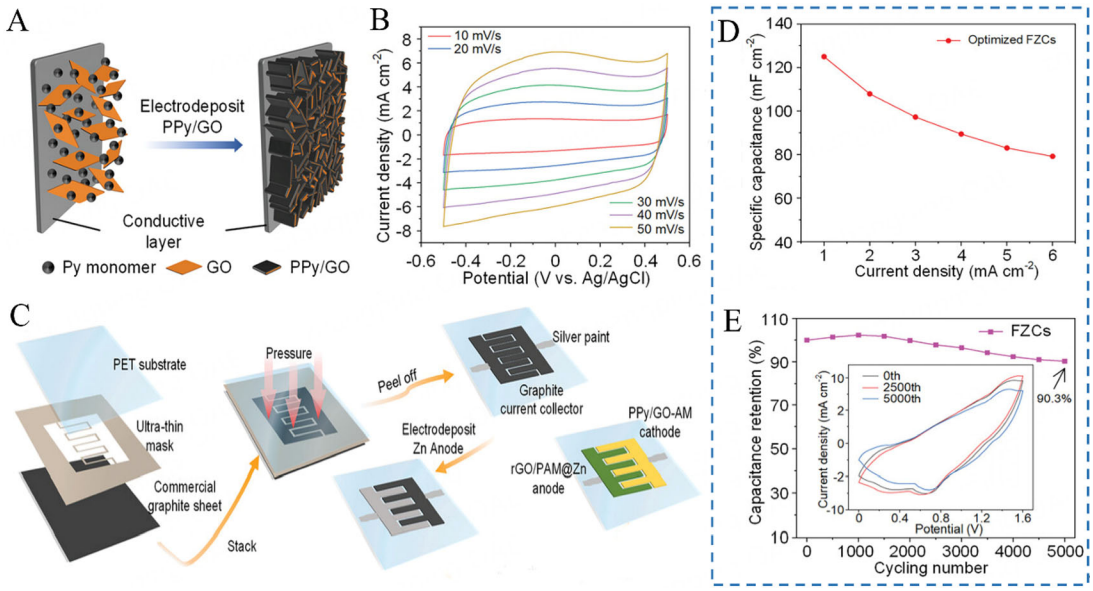

Figure 10. (A) Diagram of the fabrication of PPy/GO; (B) CV curves of PPy/GO; (C) Schematic illustration of the preparation of flexible ZHSCs with PPy/GO electrodes; (D) Areal capacitance of ZHSCs; (E) Cycling performance of device at a scan rate of 100 mV s^{-1}. Reproduced with permission from Ref.[115]. Copyright 2024, Wiley. PPy: Polypyrrole; GO: graphene oxide; CV: cyclic voltammetry; ZHSCs: zinc-ion hybrid supercapacitors.

Carbon nanosheets

Two-dimensional porous carbon nanosheets (PCNs) feature abundance of micro- to mesopores and high SSA to facilitate ion accumulation at the interface by offering numerous active sites[116-118]. Achieving an optimal thickness for PCNs is essential for effective ion transport. The appropriate thickness helps avoid the bending and aggregating of ultrathin nanosheets, reduces the length of ion migration routes, and enhances the dynamics of ion diffusion. This arrangement decreases resistance and results in a low Warburg coefficient alongside a high ion diffusion coefficient, promoting rapid transport of the electrolyte[119]. PCNs have been effectively employed as materials for electrodes, highlighting their practical significance in ZHSCs. For example, a tile-shaped carbon nanosheet (referred to as carbon tile, CT) was created by Cao *et al.*[120] from kapok and integrated with single-walled CNTs (SWNTs). This composite, exhibiting a SSA of 947 m^2 g^{-1}, facilitates short pathways for ion penetration and boasts a high ion-accessible surface area, thereby allowing reversibly ionic adsorption/desorption. The CT/SWNT ZHSC showed excellent rate capability and both gravimetric and areal performance, achieving a capacity of 114 mAh g^{-1} at a considerable mass loading of 12 mg cm^{-2}, while maintaining volumetric capacity.

Incorporating heteroatoms into PCNs can optimize the wettability, improve the electronic conductivity, and enhance the electric charge capacity. For example, Zhang *et al.*[121] designed a cathode using N and P co-doped PCNs. The introduction of N and P heteroatoms can reduce the energy threshold required for reactions involving the cathode and zinc ions, which is confirmed by the analysis of theoretical modeling. The resulting ZHSC achieved a capacitance of 232.2 F g^{-1} at 0.1 A g^{-1}; calculated energy and power densities were as high as 81.1 Wh kg^{-1} and 13.366 kW kg^{-1}, respectively. Xu *et al.*[122] prepared holey activated PCNs [holey activated carbon sheets (HACS)] originating from a low-cost molecular salt serving as an ideal precursor to fabricate HACS doped with abundant heteroatoms [Figure 11A]. The molecular salt was carbonized, self-activated, and subsequently acidic washed to convert into ACs possessing a holey sheet morphology with a remarkable SSA of 1004 m^2 g^{-1} [Figure 11B]. The obtained ACs also featured a hierarchical porosity, encompassing both micropores and mesopores, along with plentiful O (10.2 at%) and

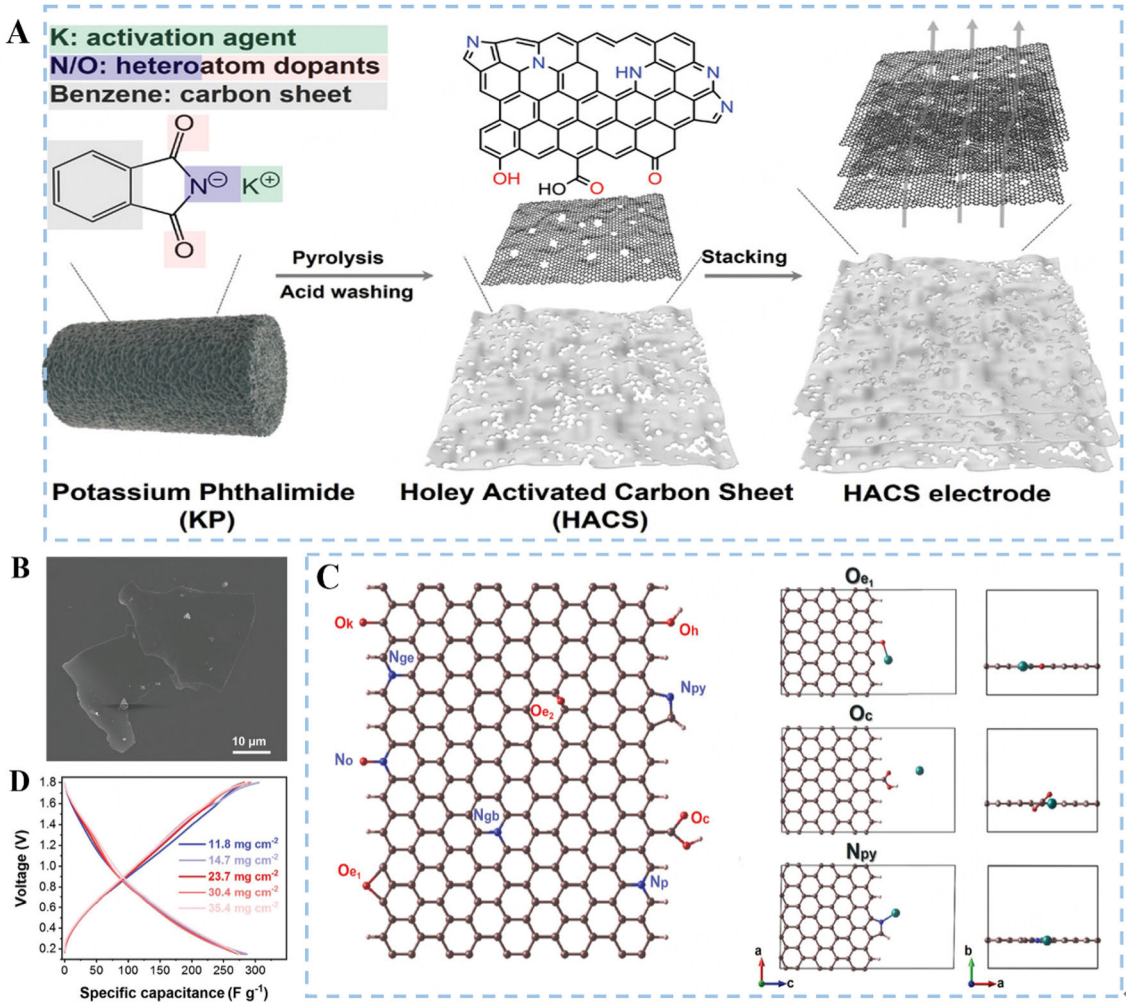

Figure 11. (A) Schematic selection of molecule and synthesis of HACS; (B) SEM images of HACS; (C) DFT calculation of HACS; (D) Charge-discharge curves of HACS cells with different mass loadings. Reproduced with permission from Ref.[122]. Copyright 2024, Wiley. HACS: Holey activated carbon sheets; SEM: scanning electron microscopy; DFT: density functional theory.

N (6.64 at%) dopants. The DFT calculations revealed that the maximum binding capability of Zn occurred on ether1 oxygen (Oe1) sites, carboxylic oxygen (Oc) and pyrrolic nitrogen (Npy) sites. The theoretic analysis suggested that the most potent adsorption energies of Oe1, Oc, and Npy could result in non-reversible ion storage [Figure 11C]. Consequently, the HACS, which is rich in these sites, could facilitate the Zn^{2+}/protons co-storage through a combination of reversible physical and chemical adsorption, as well as precipitation and dissolution during the charging and discharging cycles. Consequently, the HACS exhibited an ideal capacity retention of 68% after 27,000 cycles at 2 A g^{-1} and ≈100% Coulombic efficiency (CE). Moreover, as the mass loading augmented, HACS delivered a direct proportionality in areal capacitance, rising from 2.50 F cm^{-2} at 9.1 mg cm^{-2} to 9.00 F cm^{-2} at 35.4 mg cm^{-2} [Figure 11D].

Carbon nanosheets derived from biomass and doped with heteroatoms have emerged as a compelling subject of research due to their potential as a sustainable, cost-effective, and eco-friendly alternative for fabricating advanced cathodes. Therefore, it is essential to promote the progress of bio-renewable carbon sources and develop efficient techniques for the mass production of highly effective and stable carbon materials. Unfortunately, the intricate understanding of how various dopants and functional groups interact

synergistically and their mechanisms influencing Zn ion storage remains unclear. Wang *et al.*[123] produced the oxygen- and nitrogen-doped PCNs, utilizing the epiphytic roots of Ficus macrocarpa as a carbon precursor. These roots were carbonized through a two-stage process consisting of pyrolysis followed by activation to obtain a carbonaceous material designated as Hierarchical porous carbon nanosheets functionalized with oxygen groups and nitrogen dopants (FHPCNSs). The produced FHPCNSs carbonized at 800 °C displayed a remarkable SSA (1,454.7 $m^2 g^{-1}$) with plentiful surface compositions (O, 38.8 at%; N, 3.1 at%). The obtained CV curves revealed an extensive voltage window of 0.35 V to 2.0 V. This characteristic was linked to the suppression of oxygen and hydrogen evolution responses, attributable to the significant abundance of oxygenic and nitrogenic groups on the FHPCNSs. It was reasoned that the synergistic effects between pyrrolic-N and carboxyl functional groups on the carbon surface facilitated the adsorption of Zn^{2+} ions. Consequently, the high capacity (220.1 mAh g^{-1} at a current density of 0.2 A g^{-1}) and significant energy density (181.6 Wh kg^{-1} with a power density of 165.0 W kg^{-1}) were achieved in the assembled FHPCNSs-ZHSC.

Preparing PCN with "surface pores" requires effective methodologies. The thermal decomposition process in carbonaceous materials or those derived from biomass templates can be sustained at elevated temperatures. Nonetheless, conventional techniques face several significant challenges[124,125]. First, it is difficult to precisely regulate the defects and impurities in the biomass, leading to the inability to reproduce the pore formation consistently. Furthermore, the creation of a somewhat limited porous framework is solely achievable via the method of defect deconstruction, making it unsuitable for the HSCs that demand superior rate performance. To address these problems, researchers are concentrating on activation techniques that are both more feasible and effective. Liu *et al.*[126] followed the previously documented technique of holey graphene to develop a hierarchically PCN, utilizing the desiccated petals of Bougainvillea as a base material [Figure 12A]. Considering the features of various activation techniques, biomass-derived PCNs were synthesized through a direct process involving KOH activation and carbonization utilizing Bougainvillea petals, and the resulting nanosheets were employed as cathode materials in ZHSCs. Furthermore, essential activation parameters were examined (activation temperature and sample/KOH mass ratio) to achieve a high SSA and surface pore structure [Figure 12B and C]. It could be speculated from the *Ex-situ* high-resolution XPS spectra (depicted in Figure 12D-G) that the absorption of Zn^{2+} onto the electrode surface was able to alter O-related signal characteristics, such as their position or peak intensity. Although N-related signals might not be directly involved in Zn^{2+} storage, their presence could modify the electronic configuration of the electrode surface, thereby facilitating the absorption of ions more readily. The electrochemical evaluations revealed that the optimal samples (CB-3-850) exhibited an impressive specific capacity of 239.1 mAh g^{-1} at 0.5 A g^{-1}, along with an exceptional energy density of 213.4 Wh kg^{-1} at 0.446 kW kg^{-1}. Moreover, after undergoing 10,000 cycles, around 90% of the initial capacity was retained, indicating remarkable electrochemical stability.

Generally speaking, 2D carbon materials serve as excellent electrode materials for ZHSCs due to their well-structured pore architecture, chemical stability, favorable conductivity, and extensive theoretical SSA. The research community has been particularly concentrated on the advancement of graphene to improve the utilization efficiency of SSA, for use as cathode materials in ZHSCs. Unfortunately, the restacking and agglomeration of graphene can lead to suboptimal charge storage performance. The distinctive 2D structure of PCNs provides remarkable in-plane conductivity, facilitating the swift transfer of electrons and the flux of ions. Current research on PCNs primarily focuses on preparing materials that possess an ideal SSA and an appropriate thickness, which are crucial for achieving enhanced capacitance. Besides, these studies aim to enhance the adsorption and ion diffusion by incorporating heteroatoms to augment the number of active sites and by ensuring the presence of plentiful defects within the material.

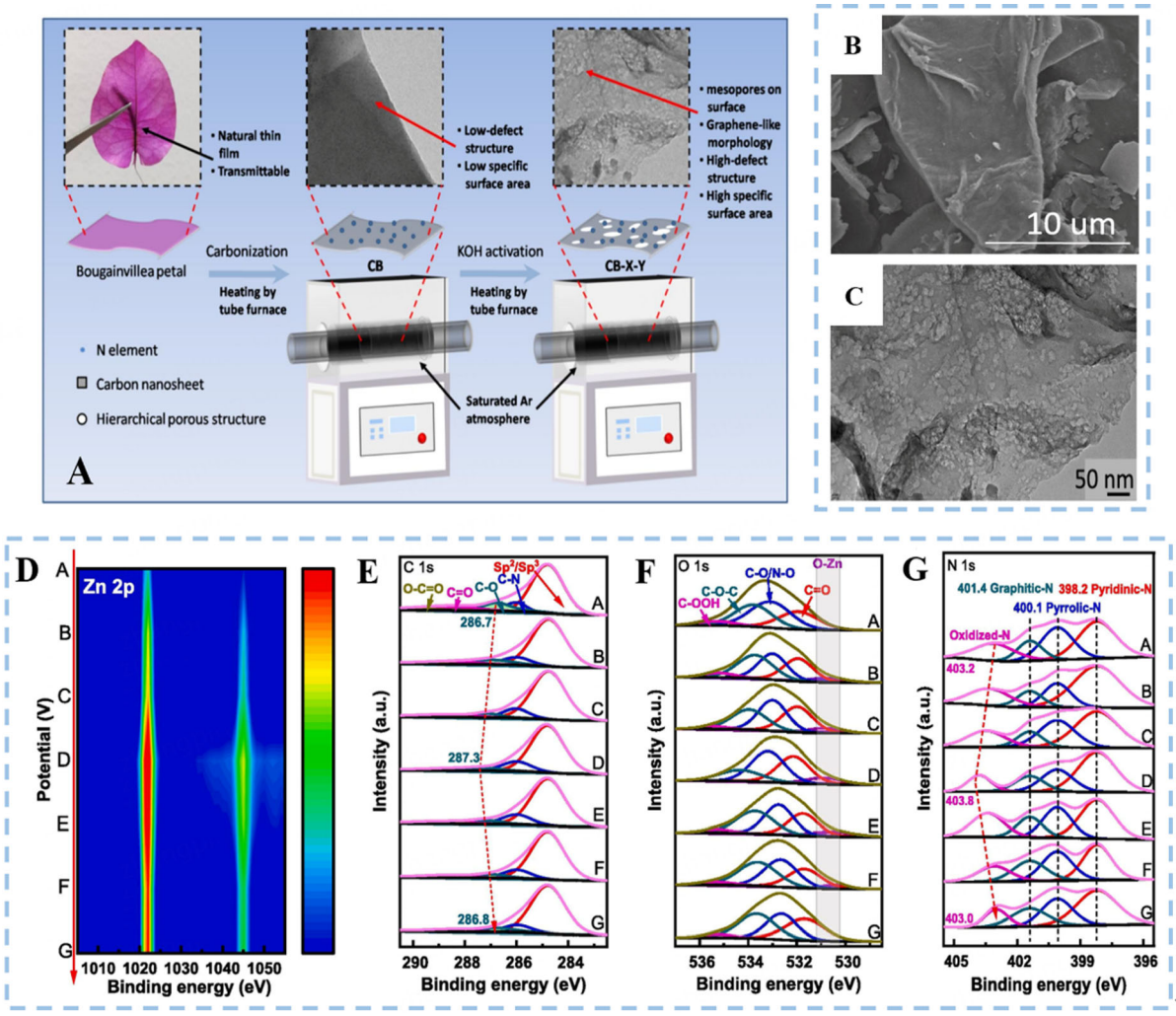

Figure 12. (A) Schematic illustration of the Synthesis of CB and CB-X-Ys; (B) SEM images and (C) High-resolution TEM (HR-TEM) images of CB-3-850; *Ex situ* high-resolution XPS spectra of (D) Zn 2p (2D contour image); (E) C 1s; (F) O 1s; and (G) N 1s for CB-3-850 cathode at different discharge-charge potentials. Reproduced with permission from Ref.[126]. Copyright 2024, Elsevier. SEM: Scanning electron microscopy; TEM: transmission electron microscopy; 2D: two-dimensional.

3D CARBONACEOUS MATERIALS

As an extensively employed electrode material of ZHSCs, 3D carbonaceous materials are adept at enhancing electron transfer and significantly reducing the diffusion path for Zn^{2+} ions to achieve rapid kinetics[127,128]. Their interconnected, continuous and tunable porosity structure increases available SSA to promote adequate contact between the electrolyte and electrode of ZHSCs, which endows the ZHSC with an impressive rate capability and power density.

3D Porous carbon

It is challenging that the low Zn^{2+} storage capacity of the 3D PC electrode stems from its energy storage mechanism, which is defined as EDLC[129]. The EDLC is significantly influenced by the SSA and the dimension of the EDL[130]. Obviously, the porosity structure regulation of 3D PC to increase the SSA is of great significance, where advanced synthesis strategies are being developed. Zeng *et al.*[131] recommended a molten salt-assisted strategy to produce a mesoporous PC (MPC) framework intended for use as a cathode. The MPC possesses high SSA of 499.31 $m^2 g^{-1}$ owing to the abundant mesopore within the structure,

resulting in an excellent capacitance (136.5 F g^{-1} at 0.68 A g^{-1}) and high cycling stability (85.4% after 10,000 cycles) for ZHSCs. Similarly, Zhang *et al.*[132] prepared porous ACs derived from pitch coke (PHC) and petroleum coke (PMC). Benefitting from the improved SSA and hierarchical porous structure, the resultant AC-PHC demonstrates a specific capacity of 146.8 mAh g^{-1} at 0.1 A g^{-1}, attractive energy density of 117 Wh kg^{-1} and power density of 15.8 kW kg^{-1}.

However, the presence of inaccessible pores and inadequate compatibility between the pore morphologies and electrolyte ions leads to a limitation in the EDLC enhancement[133]. The electrode surface containing inaccessible pores is unavailable for ion adsorption and impedes ion transport, thereby reducing the effective surface area for charge storage. Additionally, inadequate compatibility between the pore morphologies and electrolyte ions increases the resistance to ion flow, leading to higher equivalent series resistance. Shi *et al.*[134] reported an effective approach to enhance the EDLC of PC electrodes. Such enhancement was achieved by regulating the pore morphologies and diminishing the thickness of EDL via the modulation of surface charges. As illustrated in Figure 13A-C, the researchers synthesized amino group-functionalized PC materials (APCs) by pyrolyzing coal tar pitch. They further indicated that the APCs, which incorporated amino groups into the PC, demonstrated an increased charge density due to the existence of lone pair electrons. Based on the charge-density difference map, the increased negative charge density of the functionalized PC [Figure 13D and E], which could be attributed to the presence of lone pair electrons within the amino functional groups, promoted the formation of more zincophilic interfaces. Thus, the EDL in the APC was condensed [Figure 13F], which could effectively reduce the pathway of Zn^{2+} to arrive at the surface of APC and facilitate the ionic capacity. Figure 13G exhibited the CV profiles of resultant Zn//APC ZHSCs; the rectangle-shaped curves could be well preserved even at high scan rate of 100 mVs^{-1}, suggesting that these devices possessed rapid kinetics during the storage of ions and outstanding electrochemical reversibility. The Zn//APC can deliver a high capacity of 255.2 mAh g^{-1} and cycling stability of 95.5% capacity retention after 50,000 cycles for ZHSCs [Figure 13H and I]. Meanwhile, this Zn//APC ZHSC possesses a maximum energy density of 130.9 Wh kg^{-1} at 154 W kg^{-1}.

Besides porous structural and interfacial adjustment, heteroatom doping has also emerged as an indispensable method for boosting the advancement of the ZHSCs with cathodes constructed by PC. Zhang *et al.*[135] presented a modified strategy including isostatic-pressure assistance and subsequent thermal treatment to fabricate a hierarchical N-doped PC (HNPC). As for this strategy, the furfuryl alcohol and zeolite NaY were chosen as the carbon source and template, respectively. In contrast to the undoped PC, the introduction of N dopants and the multi-scale porous structure in the HNPC was credited to the linking of micropores within the PC under corrosion effect of high-temperature NH_3. Consequently, the capacity of the HNPC-based ZHSC attained 177.8 mAh g^{-1} at 4.2 A g^{-1}, and the capacitance retention could preserve 99.7% after 20,000 cycles at a current density of 16.7 A g^{-1}. Furthermore, a remarkable energy density of 107.3 Wh kg^{-1} and an ideal power density of 24.9 kW kg^{-1} are achieved. The outstanding electronical properties of HNPC-based ZHSC are partially attributed to the hierarchical porosity and improved hydrophilicity of HNPC, which accelerates ion/electron transport and provides adequate space to accommodate charge.

Currently, the derivation of heteroatom-doped PC from biomass and relevant byproducts has drawn much attention from researchers because of their well-developed porous structures, naturally occurring functional groups, and doped heteroatoms derived from intrinsic chemical structure of biomass[136-138]. Thereby, the doped PC derived from biomass can provide plentiful reaction sites and sufficient surface wettability. Li *et al.*[139] recommended a high-performance ZHSC assembled with a cathode fabricated by oxygen-enriched PC, which was obtained through the pyrolysis of olive leaves [Figure 14A]. The hierarchical porous

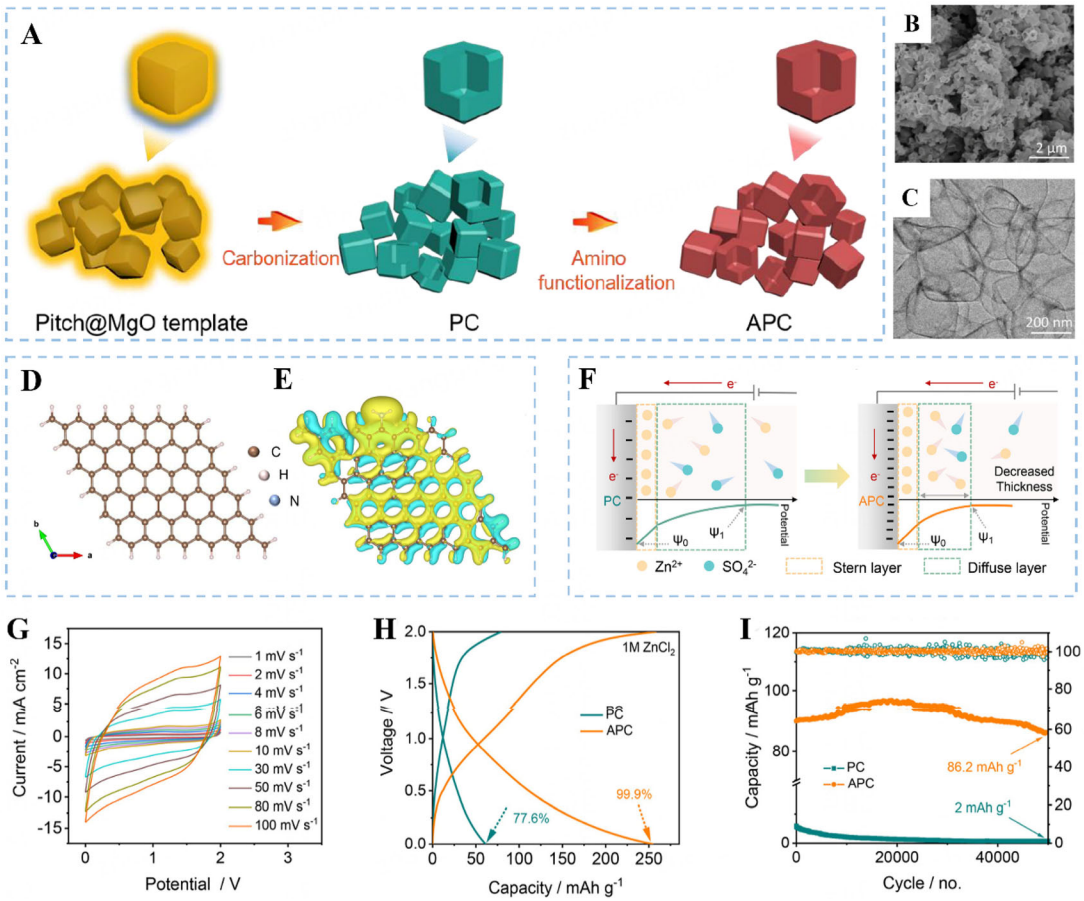

Figure 13. (A) Schematic illustration of synthesis process of APC; (B) SEM and (C) TEM images of APC; Charge-density difference map of (D) PC and (E) APC; (F) Schematic representation of the EDL configuration of PC and APC; (G) CV curves of Zn//APC ZHSCs at various scan rates; (H) GCD profiles at 0.3 A g^{-1}; (I) Cycling stability at 10 A g^{-1} of PC and APC. Reproduced with permission from Ref.[134]. Copyright 2022, Wiley. PC: Porous carbon; APC: amino group-functionalized PC material; SEM: scanning electron microscopy; TEM: transmission electron microscopy; CV: cyclic voltammetry; GCD: galvanostatic charge-discharge; ZHSCs: zinc-ion hybrid supercapacitors; EDL: electric double layer.

structure with high SSA and plentiful oxygenic groups endowed the carbon derived from the olive leaves (OLDC) with excellent chemical properties [Figure 14B and C]. The hierarchical OLDC-PC cathode, characterized by its numerous interfacial active sites and minimal ion/electron transfer distances, possessed a superior ion adsorption capacity and swift kinetics. As illustrated in Figure 14D, the contribution ratios of capacitance reached 83.1% at a scan rate of 10 mV s^{-1}, and continuously increased with the increment of the scan rates. The energy storage process, primarily governed by capacitive-driven actions, was beneficial for achieving high-performance ZHSCs that exhibit excellent rate capability and power characteristics. Therefore, an excellent energy density of 136.3 W h kg^{-1} and impressive capacity retention of 91% after 20,000 cycles at 10 A g^{-1} were achieved [Figure 14E]. Similarly, Chen *et al.*[140] developed a universal strategy for preparing chitosan-derived hierarchical PC with ant-nest-like structures defined as AH-PCs. The ammonium persulfate was utilized as an oxidant to improve the active sites of AH-PCs. Meanwhile, acetic acid facilitated the conversion of functional groups in chitosan, making them compatible for cross-linking, thereby enhancing the cross-linking degree for the efficient preparation of AH-PCs. The contribution ratio of capacitive of AH-PCs at 5 mV s^{-1} was 57%, much lower than that of OLDC-PC mentioned above. Utilizing a 6 M KOH electrolyte, the assembled ZHSC achieved an energy density of 11.44 W h kg^{-1} at 125 W kg^{-1} and a capacity retention rate of 94.9% after 400 000 cycles at 10 A g^{-1}. Researchers also attempted

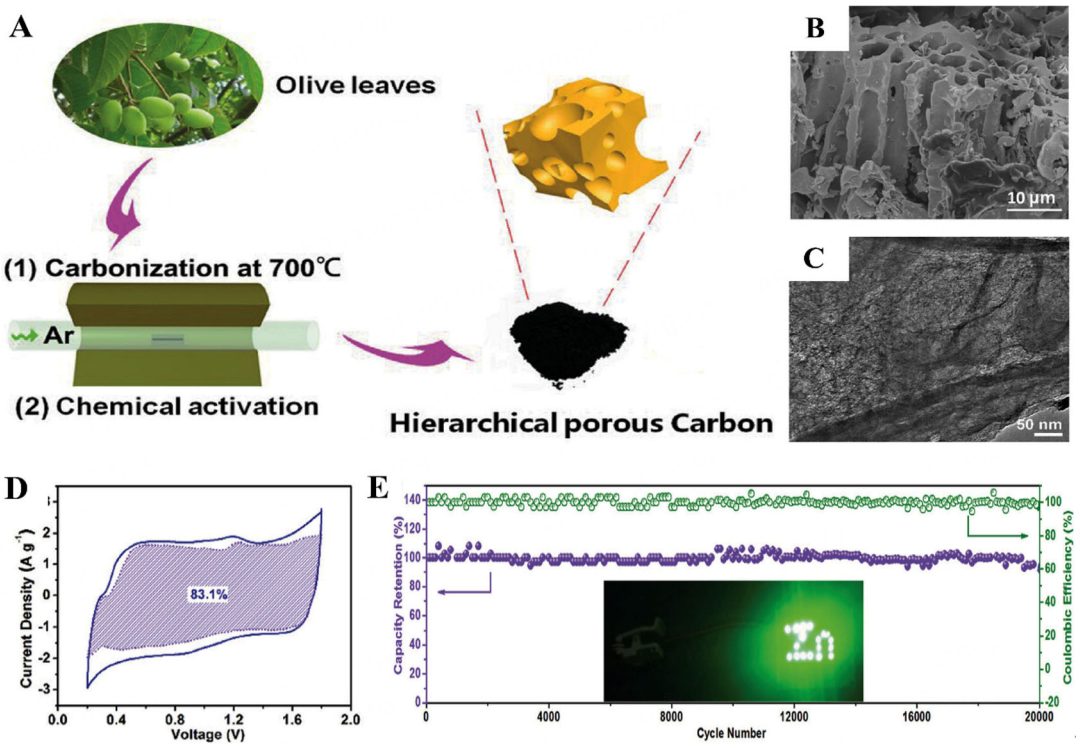

Figure 14. (A) Diagrammatic representation outlines the process of crafting hierarchical porous carbon derived from OLDC; (B) The SEM and (C) TEM images of OLDC; (D) The capacitive contribution under 10 mV s^{-1}; (E) Cycling durability at 10 A g^{-1}. Reproduced with permission from Ref.[139]. Copyright 2023, Wiley. SEM: Scanning electron microscopy; TEM: transmission electron microscopy; OLDC: carbon derived from the olive leaves.

to assemble ZHSC with 1 M Na_2SO_4 solution as the electrolyte, achieving a specific capacitance of 37.69 W h kg^{-1} and a power density of 0.225 kW kg^{-1}. Notably, the capacity retention rate of assembled ZHSC remained 100% even after 20,000 cycles.

3D graphene-based materials

Based on specific methods, 2D graphene nanosheets can interlink together as building units to perform bottom-up assembly, ultimately constituting macro 3D graphene-based materials[141-143]. The bulky structure of 3D graphene-based materials prevents the tendency to agglomerate and restack 2D graphene, preserving an appropriate SSA and enhancing the exposure of active sites. Meanwhile, the elaborate porous structure with large amounts of ion diffusion channels is efficient in shortening the length of mass transfer[144]. If the pore dimension of 3D graphene-based materials can precisely adapt the size of the Zn or hydrate ions, the maximum capacitance of ZHSCs can be achieved[145]. Most of the current research has been directed towards the development of cathodes consisting of 3D graphene-based materials with adequate SSA and hierarchical porous structures, aiming to enhance the specific capacitance. However, these porous materials always show low density arising from the excessive void, which weakens the volumetric capacitance. Therefore, the investigation of carbon materials possessing high SSA and suitable density is significant for achieving elevated volumetric energy density of ZHSCs.

Xu *et al.*[146] reported a 3D porous graphene (3D-PG-1) cathode incorporating impressive compactness and interconnected porosity. This nanomaterial was obtained through the capillary evaporation of graphene hydrogel. As shown in Figure 15A and B, the 3D-PG-1 material contracted into a rod-shaped form due to the influence of capillary evaporation, resulting in a considerably reduced volume, while the 3D-PG-2

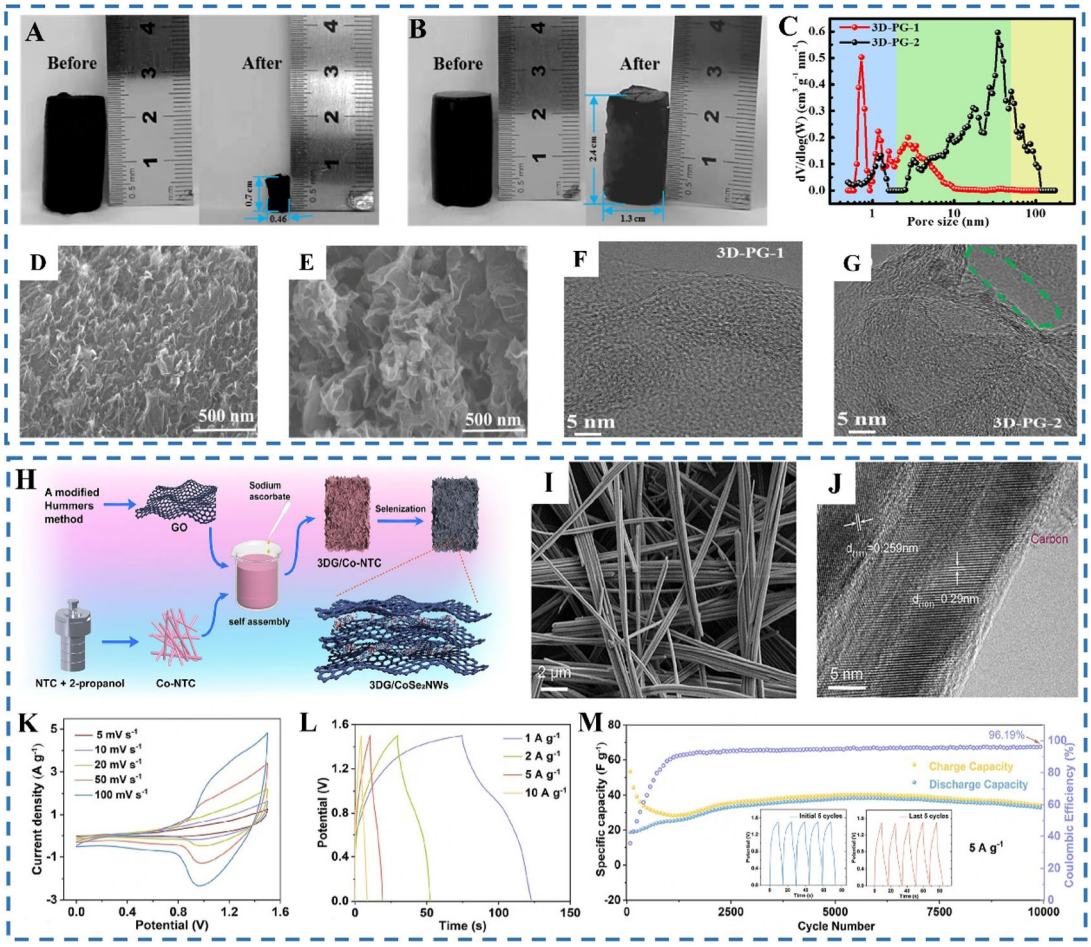

Figure 15. Field photographs of (A) 3D-PG-1 and (B) 3D-PG-2; (C) The distribution of pore sizes in 3D-PG-1 and 3D-PG-2; (D) SEM images of 3D-PG-1 and (E) 3D-PG-2; HRTEM images of (F) 3D-PG-1 and (G) 3D-PG-2. Reproduced with permission from Ref.[146]. Copyright 2022, Elsevier. (H) Schematic diagram of the preparation process of 3DG/CoSe2NWs; (I) SEM and (J) TEM images of CoSe2NWs; (K) CV curves of CoSe2NWs at different scan rates; (L) GCD curves of 3DG/CoSe2NWs at different current densities; (M) Cycling performance of the 3DG/CoSe2NWs//AC device at 5 A g^{-1} for 10,000 cycles; Reproduced with permission from Ref.[147]. Copyright 2023, American Chemical Society. 3D: Three-dimensional; PG: porous graphene; SEM: scanning electron microscopy; TEM: transmission electron microscopy; CV: cyclic voltammetry; GCD: galvanostatic charge-discharge; AC: activated carbon.

fabricated by freeze-drying without visible shrinkage of the volume. Obviously, the tap density (1.36 g cm^{-3}) and apparent density (1.38 g cm^{-3}) of 3D-PG-1 are significantly higher than those of 3D-PG-2. The 3D-PG-1 provided plentiful micropores with a size ranging from 0.6 nm to 1 nm [Figure 15C], intriguingly approximating the radius size of the hydrated Zn^{2+} ion (0.43 nm) to ensure a high capacitance of ZHSC. Thus, the electrostatic adsorption of the Zn^{2+} on the cathode material was mitigated to enable long cycling stability. The scanning electron microscopy (SEM) images showed that the nanosheets within 3D-PG-1 were compacted to obtain a tight structure with abundant interconnected pores, whereas 3D-PG-2 exhibited a looser microstructure [Figure 15D and E]. The transmission electron microscopy (TEM) image further confirmed the discrepancies in density and pore morphologies between 3D-PG-1 and 3D-PG-2 [Figure 15F and G]. The plentiful oxygenic groups of 3D-PG-1 improved not only the wetting ability of the electrolyte but also the pseudocapacitance. Therefore, the assembled ZHSC possessed outstanding specific volumetric capacitance, reaching 299 F cm^{-3} at 0.1 A g^{-1}, excellent long-term stability with an 85% capacitance retention after 30000 cycles, and a significantly volumetric energy density of 118 Wh L^{-3} at 116 W L^{-3}.

Unlike the methods of dehydrating the graphene hydrogel, 3D graphene aerogel with interconnecting network structure can also be fabricated by assembling and overlapping 1D or 2D graphene nanomaterials. Due to the hierarchical porosity, characteristic morphologies, and large contact area of 3D graphene aerogel, the device constructed by this aerogel can achieve high chemical performance and applicability. Zou *et al.*[147] proposed a simple selenization approach and delineated a flexible electrode with 3D porous nanostructures [Figure 15H]. The 1D nanowires were synthesized by coordinated Co ions and nitrilotriacetic acid in isopropanol; then, these nanowires were enwrapped in graphene with functional groups chemically reduced by sodium ascorbate. The obtained GO/Co-NTC were transformed into a 3DG/Co-NTC through self-assembly, subsequently selenized to obtain a 3DG/CoSe2NWs. In the 3DG/CoSe2NWs composite, the 3D network of interconnected pores featuring large apertures significantly enhanced the structural integrity and stability of cathode [Figure 15I and J]. Notably, the CV plots for the 3DG/CoSe2NWs electrode displayed an upward movement of the oxidation peak and a downward shift of the reduction peak, signifying rapid redox dynamics and excellent reversibility of the 3DG/CoSe2NWs material [Figure 15K]. As demonstrated in Figure 15L, there existed a direct relationship between the discharge time and the specific capacity of the material. Consequently, the flexible electrode 3DG/CoSe2NWs displayed a high reversible capacity of 1,272 F g^{-1} at 1 A g^{-1}. Notably, the capacity at 10 A g^{-1} can be maintained at 1,156 F g^{-1}, emphasizing a remarkable rate capability of 90.1% [Figure 15M]. The capacitor assembled by 3DG/CoSe2NWs//AC could maintain a steady voltage after bending, indicating great promise for practical use.

To sum up, to achieve enhanced zinc ion storage capacity in contrast to 0D, 1D and 2D carbon structures, the primary focus in developing 3D carbonaceous materials resides not merely in establishing internally interconnected architectures but also in regulating well-developed porous morphologies. It is expected that the rate capability of 3D PC can be further optimized by investigating the reasonable strategy for constructing ideal 3D structures. Among the 3D carbonaceous materials, both the graphene hydrogel and the graphene aerogel exhibit substantial structure and intricate internal porosity, which provides plentiful electrochemical active sites and accelerates mass transfer.

SUMMARY AND PERSPECTIVE

This review examines previously reported studies focused on enhancing the electrochemical performance of carbonaceous cathodes in ZHSCs. Although ZHSCs have advanced rapidly, significant scientific and technical challenges persist, particularly the scarcity of high-performance cathode materials, which impedes their ability to meet practical requirements. Carbonaceous materials, which are the predominant choice for cathodes in ZHSCs, must satisfy several criteria: high conductivity, a large SSA, exceptional chemical stability, and an appropriate pore structure. Carbonaceous materials for cathodes within ZHSCs can be categorized by their distinctive dimensions and corresponding structures, which will be briefly introduced with their benefits and drawbacks in Table 2. Moreover, the electrochemical properties of new carbonaceous materials employed in ZHSC construction are listed in Table 3. Enhancing the capacitance of carbonaceous materials can be achieved through the strategies of porous nanostructure engineering and pseudocapacitance engineering. Porous nanostructure engineering boosts capacitance by crafting a porous structure with high SSA and optimizes porosity. Additionally, pseudocapacitance engineering enhances capacity primarily through surface alterations and the incorporation of heteroatoms. These heteroatoms act as dopants, introducing a multitude of active sites within the carbon matrix, which in turn enhances the chemical adsorption on the electrode surface. The presence of Zn^{2+} ions can engage in chemical adsorption interactions with these active sites, subsequently enhancing the adsorptive capacity and the energy storage efficiency of ZHSCs. However, an elevated content of heteroatoms may result in certain sites becoming overly reactive, which can cause electrochemical instability or aggressive reactions, ultimately affecting the

Table 2. Carbonaceous structures for cathodes of ZHSCs with their benefits and drawbacks

	0D	1D	2D	3D
Benefits	◆ Controllable particle size distribution ◆ Accelerated mass transfer rate	◆ High electrical and ionic conductivity ◆ Direct electron transmission paths	◆ Enriched surface atoms or electroactive sites ◆ Unique layered structure	◆ Continuous and tunable porous structure ◆ Significantly shortened ion diffusion length
Drawbacks	◆ Unavoidable segregation effect of particles ◆ Lack of active sites	◆ Limited SSA ◆ Lack of active sites	◆ Incidental agglomeration and restack ◆ Easily damaged lamellar structure	◆ Improper pore distribution ◆ Sluggish ion diffusion within the tunnel

ZHSCs: Zinc-ion hybrid supercapacitors; SSA: specific surface areas.

Table 3. Comparison of electrochemical performance of recent carbonaceous electrode materials for ZHSCs

Dimension	Cathode	Anode	Voltage (V)	Cycling stability	Energy density (Wh kg^{-1})	Power density (kW kg^{-1})	Refs.
0D	HMCSs	HMCSs	0-1.6	99.4% (2,500 cycles)	75.4	0.16	[75]
	PDA-HCSs	Zn foil	-1.0-0	90.1% (10,000 cycles)	43.1	0.7946	[76]
	PN-CHoNS	Zn foil	0.2-1.8	80.6% (12,000 cycles)	116.0	21.66	[77]
	CS_{30}	Zn foil	0.2-1.8	96.9% (20,000 cycles)	118.3	21.3	[78]
	CDs/NZP	Zn foil	0-1.6	90.6% (6,000 cycles)	33.7	0.8249	[79]
	LVCR	Zn foil	0.2-1.8	96.9% (20,000 cycles)	126.6	31.4	[80]
1D	NP-MWCNT@GONR	NP-MWCNT@GONR//Zn	0-2.0	67.5% (2,000 cycles)	68.38	19	[88]
	CNT@PC	Zn foil	0.2-1.8	99.2% (3,0000 cycles)	74.4	40	[90]
	N-OPCNF	Zn foil	0.2-1.8	80.38% (8,000 cycles)	98.28	0.072	[104]
	MCHCNF	Zn foil	0.2-1.8	93% (15,000 cycles)	133.1	34.4	[107]
2D	aMEGO	Zn foil	0.2-1.8	93% (80,000 cycles)	106.3	31.4	[109]
	RG-R	Zn foil	0.2-1.6	94.5% (10,000 cycles)	100.9	0.007	[110]
	graphene@CC	Zn@CC	0.2-1.8	73.7 (50,000 cycles)	158.1	0.2369	[111]
	MIL-88B(V)@rGO	Zn foil	0.2-1.6	80.3% (400 cycles)	230	2.3	[114]
	PPy/GO-AM	rGO/PAM@Zn	0-1.8	90.3% (5,000 cycles)	...	...	[115]
	HACS	Zn foil	0.2-1.8	68% (27,000 cycles)	149.6	0.0338	[122]
	FHPCNSs	Zn foil	0.35-2.0	94.5% (10,000 cycles)	181.6	0.165	[123]
	CB-3-850	Zn foil	0-1.8	90% (10,000 cycles)	213.4	0.4463	[126]
3D	AC-PHC	Zn foil	0-1.9	58% (10,000 cycles)	117	15.8	[132]
	APC	Zn foil	0-2.0	95.5% (50,000 cycles)	130.9	154	[134]
	HNPC	Zn foil	0-2.0	99.7% (20,000 cycles)	107.3	24.9	[135]
	OLDC	Zn foil	-3.0-1.0	91% (20,000 cycles)	37.69	0.225	[139]
	3D-PG-1	Zn foil	0.2-1.8	85% (30,000 cycles)	118	0.156	[146]
	3DG/CoSe2NWs	Zn foil	0-1.5	96.19% (10,000 cycles)	10.2	0.75	[147]

ZHSCs: Zinc-ion hybrid supercapacitors; PDA: polydopamine; HCSs: hollow carbon spheres; PN-CHoNS: P/N dual-doped hollow carbon spheres; CNTs: carbon nanotubes; PC: porous carbon; N-OPCNF: Nanosheets onto a arbon nanofiber framework; rGO: reduced graphene oxide; RG-R: rGO foam; PPy: polypyrrole; AM: acrylamide; HACS: holey activated carbon sheets; AC-PHC: activated carbon-pitch coke; PC: porous carbon; APC: amino group-functionalized PC material; HNPC: hierarchical N-doped PC; HMCSs: hollow mesoporous carbon spheres; CDs/NZP: carbon nanodots with Ni-Zn phosphates; LVCR: hierarchical micro-, meso-and macropores; NP-MWCNT@GONR: nanoporous multi-wall carbon nanotube@graphene oxide nanoribbons; MCHCNF: multi-channel hollow carbon nanofiber; aMEGO: porous carbon derived from chemical activated graphene; FHPCNSs: hierarchical porous carbon nanosheets functionalized with oxygen groups and nitrogen dopants.

cycling life and electrochemical stability of ZHSCs. Furthermore, it is crucial to explore the correlation between the purity of carbonaceous materials and the electrochemical performance in ZHSCs. This document outlines the challenges associated with carbonaceous cathodes in ZHSCs and provides insights

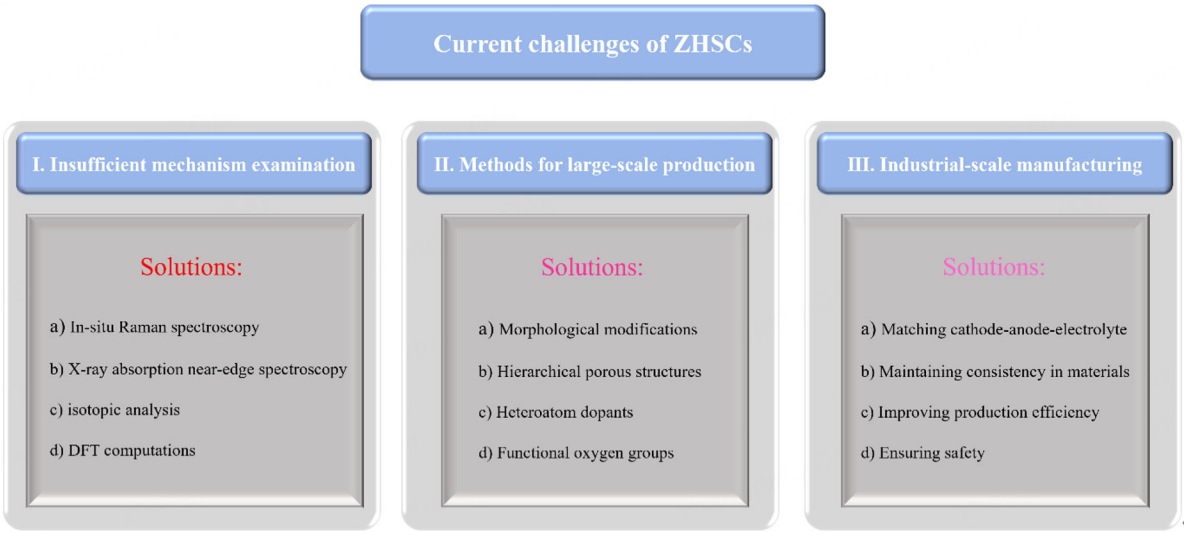

Figure 16. Challenges and solutions for the advancement in ZHSCs proposed for future research. ZHSCs: Zinc-ion hybrid supercapacitors.

into future development for ZHSCs, which are summarized in Figure 16, along with the following details:

The examination of the electrochemical mechanism lacks sufficient depth. Beyond basic ion adsorption/desorption processes within the EDL, the electrochemical characteristics of carbonaceous cathodes require further validation through various advanced characterization techniques, electrochemical analyses, and theoretical assessments. *In-situ* spectroscopy can be employed to investigate the chemical states of other elements (C, O, or H), thereby enabling an indirect analysis of Zn^{2+}. Additionally, it is highly advisable to employ methods such as X-ray absorption near-edge spectroscopy, DFT computations, and isotopic analysis. Furthermore, the generality of chemical adsorption onto the electrode surface, coupled with the impact of side reactions on overall performance, continues to be a matter of debate that requires further investigation. This research will enhance the understanding of the energy storage mechanisms in ZHSCs, ultimately aimed at intentionally improving their capacitance and energy density.

The advancement of high-performance carbon-based materials and the investigation of effective methods for large-scale production are critical research domains. Future studies should concentrate on designing innovative high-performance cathode materials, building on current theoretical models. To date, researchers have made substantial efforts employing techniques such as morphological modifications, the creation of hierarchical porous structures, doping with heteroatoms, and the incorporation of functional oxygen groups. However, maintaining precise control over the doping of heteroatoms remains a significant challenge for future research. Additionally, the modifications involving the introduction of heteroatoms or oxygen functional groups can significantly impact energy density, conductivity, and crystallinity. In contrast, various nitrogen species in carbon materials fulfill distinct roles, with optimal performance achieved through a careful balance of their concentrations. Therefore, pursuing a balanced approach to the diverse physical and chemical properties of carbon electrodes through systematic exploration of modification strategies is an essential area of research.

Transitioning from laboratory-scale production to industrial-scale manufacturing presents significant challenges, especially in maintaining consistency in product quality, improving production efficiency, and ensuring safety during large-scale processes. For instance, the advancement of flexible ZHSCs holds

immense scientific importance for powering wearable electronic devices. Thus, it is essential to create flexible electrodes that facilitate strong interactions between the active materials and the substrate, preventing debonding when subjected to external mechanical forces. Moreover, other devices such as microdevices, coin-sized devices, and temperature-resistant systems are also anticipated to be key research areas in the future to meet the growing energy demands and diverse application sectors.

DECLARATIONS

Authors' contributions

Literature review, data collection and writing: Cai, S.
Conceptualization, writing, and supervision: Lu, X.
Article polishing and figure design: Zhou, X.
Supervision and funding: Wang, Y.

Availability of data and materials

Not applicable.

Financial support and sponsorship

This work was supported by the Guizhou Provincial Basic Research Program (Natural Science) (No. QianKeHe Basic-[2024] Youth 085)

Conflicts of interest

Zhou, X. is affiliated with Daqing Oilfield Design Institute Co., Ltd., while the other authors have declared that they have no conflicts of interest.

Ethical approval and consent to participate

Not applicable.

Consent for publication

Not applicable.

REFERENCES

1. Shao, Y.; El-Kady, M. F.; Sun, J.; et al. Design and mechanisms of asymmetric supercapacitors. *Chem. Rev.* **2018**, *118*, 9233-80. DOI
2. Chu, S.; Majumdar, A. Opportunities and challenges for a sustainable energy future. *Nature* **2012**, *488*, 294-303. DOI PubMed
3. Huang, Y.; Wang, Y.; Tang, C.; et al. Atomic modulation and structure design of carbons for bifunctional electrocatalysis in metal-air batteries. *Adv. Mater.* **2019**, *31*, 1803800. DOI
4. Cano, Z. P.; Banham, D.; Ye, S.; et al. Batteries and fuel cells for emerging electric vehicle markets. *Nat. Energy.* **2018**, *3*, 279-89. DOI
5. Borghei, M.; Lehtonen, J.; Liu, L.; Rojas, O. J. Advanced biomass-derived electrocatalysts for the oxygen reduction reaction. *Adv. Mater.* **2018**, *30*, 1703691. DOI PubMed
6. Zhong, Y.; Xu, X.; Liu, P.; et al. A function-separated design of electrode for realizing high-performance hybrid zinc battery. *Adv. Energy. Mater.* **2020**, *10*, 2002992. DOI
7. Wan, F.; Zhang, Y.; Zhang, L.; et al. Reversible oxygen redox chemistry in aqueous zinc-ion batteries. *Angew. Chem. Int. Ed.* **2019**, *58*, 7062-7. DOI
8. Qian, J.; Wu, C.; Cao, Y.; et al. Prussian blue cathode materials for sodium-ion batteries and other ion batteries. *Adv. Energy. Mater.* **2018**, *8*, 1702619. DOI
9. Li, J.; Chen, S.; Yang, N.; et al. Ultrahigh-loading zinc single-atom catalyst for highly efficient oxygen reduction in both acidic and alkaline media. *Angew. Chem. Int. Ed.* **2019**, *131*, 7109-13. DOI

10. Wu, F.; Yang, H.; Bai, Y.; Wu, C. Paving the path toward reliable cathode materials for aluminum-ion batteries. *Adv. Mater.* **2019**, *31*, 1806510. DOI
11. Zhao, Z.; Zhao, J.; Hu, Z.; et al. Long-life and deeply rechargeable aqueous Zn anodes enabled by a multifunctional brightener-inspired interphase. *Energy. Environ. Sci.* **2019**, *12*, 1938-49. DOI
12. Lv, T.; Liu, M.; Zhu, D.; Gan, L.; Chen, T. Nanocarbon-based materials for flexible all-solid-state supercapacitors. *Adv. Mater.* **2018**, *30*, 1705489. DOI
13. Da, Y.; Liu, J.; Zhou, L.; Zhu, X.; Chen, X.; Fu, L. Engineering 2D architectures toward high-performance micro-supercapacitors. *Adv. Mater.* **2019**, *31*, 1802793. DOI
14. Ren, Q.; Wang, H.; Lu, X. F.; Tong, Y. X.; Li, G. R. Recent progress on MOF-derived heteroatom-doped carbon-based electrocatalysts for oxygen reduction reaction. *Adv. Sci.* **2018**, *5*, 1700515. DOI
15. Qiu, H. J.; Du, P.; Hu, K.; et al. Metal and nonmetal codoped 3D nanoporous graphene for efficient bifunctional electrocatalysis and rechargeable Zn-air batteries. *Adv. Mater.* **2019**, *31*, 1900843. DOI
16. Yang, Y.; Tang, Y.; Fang, G.; et al. Li^+ intercalated $V_2O_5{\cdot}nH_2O$ with enlarged layer spacing and fast ion diffusion as an aqueous zinc-ion battery cathode. *Energy. Environ. Sci.* **2018**, *11*, 3157-62. DOI
17. Lethien, C.; Le, B. J.; Brousse, T. Challenges and prospects of 3D micro-supercapacitors for powering the internet of things. *Energy. Environ. Sci.* **2019**, *12*, 96-115. DOI
18. Guo, W.; Yu, C.; Li, S.; et al. Strategies and insights towards the intrinsic capacitive properties of MnO_2 for supercapacitors: challenges and perspectives. *Nano. Energy.* **2019**, *57*, 459-72. DOI
19. Li, B.; Zheng, J.; Zhang, H.; et al. Electrode materials, electrolytes, and challenges in nonaqueous lithium-ion capacitors. *Adv. Mater.* **2018**, *30*, 1705670. DOI
20. Jiang, J.; Li, Y.; Liu, J.; Huang, X.; Yuan, C.; Lou, X. W. Recent advances in metal oxide-based electrode architecture design for electrochemical energy storage. *Adv. Mater.* **2012**, *24*, 5166-80. DOI
21. Choi, J. W.; Aurbach, D. Promise and reality of post-lithium-ion batteries with high energy densities. *Nat. Rev. Mater.* **2016**, *1*, 1-6. DOI
22. Zhang, L. L.; Zhao, X. S. Carbon-based materials as supercapacitor electrodes. *Chem. Soc. Rev.* **2009**, *38*, 2520-31. DOI PubMed
23. Yang, C.; Chen, J.; Ji, X.; et al. Aqueous Li-ion battery enabled by halogen conversion-intercalation chemistry in graphite. *Nature* **2019**, *569*, 245-50. DOI
24. Jiang, H.; Lee, P. S.; Li, C. 3D carbon based nanostructures for advanced supercapacitors. *Energy. Environ. Sci.* **2013**, *6*, 41-53. DOI
25. Huang, J.; Sumpter, B.; Meunier, V. Theoretical model for nanoporous carbon supercapacitors. *Angew. Chem. Int. Ed.* **2008**, *120*, 530-4. DOI PubMed
26. Kang, B.; Ceder, G. Battery materials for ultrafast charging and discharging. *Nature* **2009**, *458*, 190-3. DOI PubMed
27. Lukatskaya, M. R.; Dunn, B.; Gogotsi, Y. Multidimensional materials and device architectures for future hybrid energy storage. *Nat. Commun.* **2016**, *7*, 12647. DOI PubMed PMC
28. Dong, L.; Ma, X.; Li, Y.; et al. Extremely safe, high-rate and ultralong-life zinc-ion hybrid supercapacitors. *Energy. Storage. Mater.* **2018**, *13*, 96-102. DOI
29. Zuo, W.; Li, R.; Zhou, C.; Li, Y.; Xia, J.; Liu, J. Battery-supercapacitor hybrid devices: recent progress and future prospects. *Adv. Sci.* **2017**, *4*, 1600539. DOI
30. Dong, L.; Yang, W.; Yang, W.; Li, Y.; Wu, W.; Wang, G. Multivalent metal ion hybrid capacitors: a review with a focus on zinc-ion hybrid capacitors. *J. Mater. Chem. A.* **2019**, *7*, 13810-32. DOI
31. Boruah, B. D. Roadmap of in-plane electrochemical capacitors and their advanced integrated systems. *Energy. Storage. Mater.* **2019**, *21*, 219-39. DOI
32. Fu, W.; Zhao, E.; Ma, R.; et al. Anatase TiO_2 confined in carbon nanopores for high-energy Li-ion hybrid supercapacitors operating at high rates and subzero temperatures. *Adv. Energy. Mater.* **2020**, *10*, 1902993. DOI
33. Tie, D.; Huang, S.; Wang, J.; Ma, J.; Zhang, J.; Zhao, Y. Hybrid energy storage devices: Advanced electrode materials and matching principles. *Energy. Storage. Mater.* **2019**, *21*, 22-40. DOI
34. Muzaffar, A.; Ahamed, M. B.; Deshmukh, K.; Thirumalai, J. A review on recent advances in hybrid supercapacitors: Design, fabrication and applications. *Renew. Sustain. Energy. Rev.* **2019**, *101*, 123-45. DOI
35. Chen, Q.; Jin, J.; Kou, Z.; et al. Zn^{2+} pre-intercalation stabilizes the tunnel structure of MnO_2 Nanowires and enables zinc-ion hybrid supercapacitor of battery-level energy density. *Small* **2020**, *16*, 2000091. DOI
36. Zhong, Y.; Xu, X.; Veder, J. P.; Shao, Z. Self-recovery chemistry and cobalt-catalyzed electrochemical deposition of cathode for boosting performance of aqueous zinc-ion batteries. *iScience* **2020**, *23*, 100943. DOI PubMed PMC
37. Liu, C.; Wu, J. C.; Zhou, H.; et al. Great enhancement of carbon energy storage through narrow pores and hydrogen-containing functional groups for aqueous Zn-ion hybrid supercapacitor. *Molecules* **2019**, *24*, 2589. DOI PubMed PMC
38. Ma, X.; Cheng, J.; Dong, L.; et al. Multivalent ion storage towards high-performance aqueous zinc-ion hybrid supercapacitors. *Energy. Storage. Mater.* **2019**, *20*, 335-42. DOI
39. Yin, J.; Zhang, W.; Alhebshi, N. A.; Salah, N.; Alshareef, H. N. Electrochemical zinc ion capacitors: fundamentals, materials, and systems. *Adv. Energy. Mater.* **2021**, *11*, 2100201. DOI
40. Miao, L.; Lv, Y.; Zhu, D.; Li, L.; Gan, L.; Liu, M. Recent advances in zinc-ion hybrid energy storage: coloring high-power capacitors with battery-level energy. *Chin. Chem. Lett.* **2023**, *34*, 107784. DOI

41. Li, Z.; Chen, D.; An, Y.; et al. Flexible and anti-freezing quasi-solid-state zinc ion hybrid supercapacitors based on pencil shavings derived porous carbon. *Energy. Storage. Mater.* **2020**, *28*, 307-14. DOI
42. Wang, H.; Wang, M.; Tang, Y. A novel zinc-ion hybrid supercapacitor for long-life and low-cost energy storage applications. *Energy. Storage. Mater.* **2018**, *13*, 1-7. DOI
43. Zheng, Y.; Zhao, W.; Jia, D.; et al. Porous carbon prepared via combustion and acid treatment as flexible zinc-ion capacitor electrode material. *Chem. Eng. J.* **2020**, *387*, 124161. DOI
44. Yu, P.; Zeng, Y.; Zeng, Y.; et al. Achieving high-energy-density and ultra-stable zinc-ion hybrid supercapacitors by engineering hierarchical porous carbon architecture. *Electrochim. Acta.* **2019**, *327*, 134999. DOI
45. Tong, Y.; Wu, Y.; Liu, Z.; Yin, Y.; Sun, Y.; Li, H. Fabricating multi-porous carbon anode with remarkable initial coulombic efficiency and enhanced rate capability for sodium-ion batteries. *Chin. Chem. Lett.* **2023**, *34*, 107443. DOI
46. Liu, X.; Tong, Y.; Wu, Y.; et al. Synergistically enhanced electrochemical performance using nitrogen, phosphorus and sulfur tri-doped hollow carbon for advanced potassium ion storage device. *Chem. Eng. J.* **2022**, *431*, 133986. DOI
47. Liu, X.; Yu, X.; Tong, Y.; et al. Potassium storage in bismuth nanoparticles embedded in N-doped porous carbon facilitated by ether-based electrolyte. *Chem. Eng. J.* **2022**, *446*, 137329. DOI
48. Devi, N.; Sahoo, S.; Kumar, R.; Singh, R. K. A review of the microwave-assisted synthesis of carbon nanomaterials, metal oxides/hydroxides and their composites for energy storage applications. *Nanoscale* **2021**, *13*, 11679-711. DOI
49. Gautam, M.; Patodia, T.; Gupta, V.; Sachdev, K.; Kushwaha, H. S. Synthesis of high surface area activated carbon from banana peels biomass for zinc-ion hybrid super-capacitor. *J. Energy. Storage.* **2024**, *102*, 114088. DOI
50. Lin, Y.; Li, F.; Zhang, Q.; Liu, G.; Xue, C. Controllable preparation of green biochar based high-performance supercapacitors. *Ionics* **2022**, *28*, 2525-61. DOI
51. Li, Z.; Guo, D.; Liu, Y.; Wang, H.; Wang, L. Recent advances and challenges in biomass-derived porous carbon nanomaterials for supercapacitors. *Chem. Eng. J.* **2020**, *397*, 125418. DOI
52. Zhou, Y.; Luo, J.; Shao, Y.; Xia, Z.; Shao, Y. Progress on carbonene-based materials for Zn-ion hybrid supercapacitors. *New. Carbon. Mater.* **2022**, *37*, 918-35. DOI
53. Tian, Y.; Amal, R.; Wang, D. An aqueous metal-ion capacitor with oxidized carbon nanotubes and metallic zinc electrodes. *Front. Energy. Res.* **2016**, 4. DOI
54. Huang, J.; Wang, Z.; Hou, M.; et al. Polyaniline-intercalated manganese dioxide nanolayers as a high-performance cathode material for an aqueous zinc-ion battery. *Nat. Commun.* **2018**, *9*, 2906. DOI PubMed PMC
55. Han, Q.; Chi, X.; Liu, Y.; et al. An inorganic salt reinforced Zn^{2+}-conducting solid-state electrolyte for ultra-stable Zn metal batteries. *J. Mater. Chem. A.* **2019**, *7*, 22287-95. DOI
56. Liu, Y.; Zhou, X.; Liu, R.; et al. Tailoring three-dimensional composite architecture for advanced zinc-ion batteries. *ACS. Appl. Mater. Interfaces.* **2019**, *11*, 19191-9. DOI
57. Yu, L.; Li, J.; Ahmad, N.; et al. Recent progress on carbon materials for emerging zinc-ion hybrid capacitors. *J. Mater. Chem. A.* **2024**, *12*, 9400-20. DOI
58. Huang, J.; Sumpter, B. G.; Meunier, V.; Yushin, G.; Portet, C.; Gogotsi, Y. Curvature effects in carbon nanomaterials: exohedral versus endohedral supercapacitors. *J. Mater. Res.* **2010**, *25*, 1525-31. DOI
59. Wei, J.; Zhong, L.; Xia, H.; et al. Metal-ion oligomerization inside electrified carbon micropores and its effect on capacitive charge storage. *Adv. Mater.* **2022**, *34*, 2107439. DOI
60. Liu, Q.; Zhang, H.; Xie, J.; Liu, X.; Lu, X. Recent progress and challenges of carbon materials for Zn-ion hybrid supercapacitors. *Carbon. Energy.* **2020**, *2*, 521-39. DOI
61. Jin, J.; Geng, X.; Chen, Q.; Ren, T. L. A better Zn-ion storage device: recent progress for zn-ion hybrid supercapacitors. *Nanomicro. Lett.* **2022**, *14*, 64. DOI PubMed PMC
62. Zheng, J.; Wu, Y.; Sun, Y.; Rong, J.; Li, H.; Niu, L. Advanced anode materials of potassium ion batteries: from zero dimension to three dimensions. *Nanomicro. Lett.* **2020**, *13*, 1-37. DOI PubMed PMC
63. Liu, T.; Jiang, C.; Cheng, B.; You, W.; Yu, J. Hierarchical NiS/N-doped carbon composite hollow spheres with excellent supercapacitor performance. *J. Mater. Chem. A.* **2017**, *5*, 21257-65. DOI
64. Wang, J.; Liu, H.; Sun, H.; et al. One-pot synthesis of nitrogen-doped ordered mesoporous carbon spheres for high-rate and long-cycle life supercapacitors. *Carbon* **2018**, *127*, 85-92. DOI
65. Liu, J.; Wickramaratne, N. P.; Qiao, S. Z.; Jaroniec, M. Molecular-based design and emerging applications of nanoporous carbon spheres. *Nat. Mater.* **2015**, *14*, 763-74. DOI PubMed
66. Ding, J.; Zhang, H.; Zhou, H.; et al. Sulfur-grafted hollow carbon spheres for potassium-ion battery anodes. *Adv. Mater.* **2019**, *31*, 1900429. DOI
67. Yu, X.; Li, W.; Hu, Y.; Ye, C.; Lu, A. Sculpturing solid polymer spheres into internal gridded hollow carbon spheres under controlled pyrolysis micro-environment. *Nano. Res.* **2021**, *14*, 1565-73. DOI
68. Du, J.; Liu, L.; Yu, Y.; Lv, H.; Zhang, Y.; Chen, A. Confined pyrolysis for direct conversion of solid resin spheres into yolk-shell carbon spheres for supercapacitor. *J. Mater. Chem. A.* **2019**, *7*, 1038-44. DOI
69. Zhang, Y.; Sun, K.; Liang, Z.; Wang, Y.; Ling, L. N-doped yolk-shell hollow carbon sphere wrapped with graphene as sulfur host for high-performance lithium-sulfur batteries. *Appl. Surf. Sci.* **2018**, *427*, 823-9. DOI
70. Gong, J.; Liu, J.; Chen, X.; et al. One-pot synthesis of core/shell Co@C spheres by catalytic carbonization of mixed plastics and their

application in the photo-degradation of Congo red. *J. Mater. Chem. A.* **2014**, *2*, 7461-70. DOI

71. Chen, B.; Yang, L.; Bai, X.; et al. Heterostructure engineering of core-shelled Sb@Sb_2O_3 encapsulated in 3D N-doped carbon hollow-spheres for superior sodium/potassium storage. *Small* **2021**, *17*, 2006824. DOI
72. Li, S.; Zhu, H.; Liu, Y.; et al. Codoped porous carbon nanofibres as a potassium metal host for nonaqueous K-ion batteries. *Nat. Commun.* **2022**, *13*, 4911. DOI PubMed PMC
73. Park, S.; Seo, B.; Shin, D.; Kim, K.; Choi, W. Sodium-chloride-assisted synthesis of nitrogen-doped porous carbon shells via one-step combustion waves for supercapacitor electrodes. *Chem. Eng. J.* **2022**, *433*, 134486. DOI
74. Zheng, J.; Wu, Y.; Tong, Y.; et al. High capacity and fast kinetics of potassium-ion batteries boosted by nitrogen-doped mesoporous carbon spheres. *Nano-Micro. Lett.* **2021**, *13*, 174. DOI PubMed PMC
75. Chen, S.; Yang, G.; Zhao, X.; et al. Hollow mesoporous carbon spheres for high performance symmetrical and aqueous zinc-ion hybrid supercapacitor. *Front. Chem.* **2020**, *8*, 663. DOI PubMed PMC
76. Du, J.; Han, Q.; Chen, Y.; Peng, M.; Xie, L.; Chen, A. Micro/meso-porous double-shell hollow carbon spheres through spatially confined pyrolysis for supercapacitors and zinc-ion capacitor. *Angew. Chem. Int. Ed.* **2024**, *63*, e202411066. DOI
77. Li, J.; Zhang, J.; Yu, L.; et al. Dual-doped carbon hollow nanospheres achieve boosted pseudocapacitive energy storage for aqueous zinc ion hybrid capacitors. *Energy. Storage. Mater.* **2021**, *42*, 705-14. DOI
78. Song, Z.; Miao, L.; Ruhlmann, L.; et al. Lewis pair interaction self-assembly of carbon superstructures harvesting high-energy and ultralong-life zinc-ion storage. *Adv. Funct. Mater.* **2022**, *32*, 2208049. DOI
79. Guo, M.; Wang, S.; Zhao, L.; Guo, Z. High-performance asymmetric supercapacitor based on flowery nickel-zinc phosphate microspheres with carbon dots. *Electrochim. Acta.* **2018**, *292*, 299-308. DOI
80. Xiao, K.; Jiang, X.; Zeng, S.; et al. Porous structure-electrochemical performance relationship of carbonaceous electrode-based zinc ion capacitors. *Adv. Funct. Mater.* **2024**, *34*, 2405830. DOI
81. Liu, C.; Wang, J.; Li, J.; et al. Controllable synthesis of functional hollow carbon nanostructures with dopamine as precursor for supercapacitors. *ACS. Appl. Mater. Interfaces.* **2015**, *7*, 18609-17. DOI
82. Tschannen, C. D.; Frimmer, M.; Vasconcelos, T. L.; Shi, L.; Pichler, T.; Novotny, L. Tip-enhanced stokes-anti-stokes scattering from carbyne. *Nano. Lett.* **2022**, *22*, 3260-5. DOI PubMed PMC
83. Chen, X.; Zhang, H.; Gao, Y.; et al. Zinc-ion hybrid supercapacitors: design strategies, challenges, and perspectives. *Carbon. Neutraliz.* **2022**, *1*, 159-88. DOI
84. Gao, T.; Yan, G.; Yang, X.; et al. Wet spinning of fiber-shaped flexible Zn-ion batteries toward wearable energy storage. *J. Energy. Chem.* **2022**, *71*, 192-200. DOI
85. Iijima, S. Helical microtubules of graphitic carbon. *Nature* **1991**, *354*, 56-8. DOI
86. Chen, C.; Zhang, Y.; Li, Y.; et al. Highly conductive, lightweight, low-tortuosity carbon frameworks as ultrathick 3D current collectors. *Adv. Energy. Mater.* **2017**, *7*, 1700595. DOI
87. Zhang, X.; Pei, Z.; Wang, C.; et al. Flexible zinc-ion hybrid fiber capacitors with ultrahigh energy density and long cycling life for wearable electronics. *Small* **2019**, *15*, 1903817. DOI
88. Lin, W.; Liu, S.; Gull, S.; et al. Nanoporous core-shell-structured multi-wall carbon nanotube/graphene oxide nanoribbons as cathodes and protection layer for aqueous zinc-ion capacitors: mechanism study of zinc dendrite suppression by in-situ transmission X-ray microscopy. *J. Power. Sources.* **2022**, *541*, 231627. DOI
89. Wang, Q.; Yan, J.; Fan, Z. Carbon materials for high volumetric performance supercapacitors: design, progress, challenges and opportunities. *Energy. Environ. Sci.* **2016**, *9*, 729-62. DOI
90. Yang, B.; Zhao, W.; Gao, Z.; et al. Flexible CNT@Porous carbon sponge cathode with large mesopores for high-rate zinc-ion hybrid capacitors. *Carbon* **2024**, *218*, 118695. DOI
91. Tang, X.; Zhou, H.; Cai, Z.; et al. Generalized 3D printing of graphene-based mixed-dimensional hybrid aerogels. *ACS. Nano.* **2018**, *12*, 3502-11. DOI
92. Tagliaferri, S.; Nagaraju, G.; Panagiotopoulos, A.; et al. Aqueous inks of pristine graphene for 3D printed microsupercapacitors with high capacitance. *ACS. Nano.* **2021**, *15*, 15342-53. DOI PubMed PMC
93. Yang, W.; Yang, J.; Byun, J. J.; et al. 3D printing of freestanding MXene architectures for current-collector-free supercapacitors. *Adv. Mater.* **2019**, *31*, 1902725. DOI
94. Fan, Z.; Jin, J.; Li, C.; et al. 3D-printed Zn-ion hybrid capacitor enabled by universal divalent cation-gelated additive-free Ti_3C_2 MXene ink. *ACS. Nano.* **2021**, *15*, 3098-107. DOI
95. Shen, K.; Ding, J.; Yang, S. 3D printing quasi-solid-state asymmetric micro-supercapacitors with ultrahigh areal energy density. *Adv. Energy. Mater.* **2018**, *8*, 1800408. DOI
96. Xu, N.; Yan, C.; He, W.; et al. Flexible electrode material of V_2O_5 carbon fiber cloth for enhanced zinc ion storage performance in flexible zinc-ion battery. *J. Power. Sources.* **2022**, *533*, 231358. DOI
97. kumar T, Babu KJ, Yoo DJ, Kim AR, Gnana kumar G. Binder free and free-standing electrospun membrane architecture for sensitive and selective non-enzymatic glucose sensors. *RSC. Adv.* **2015**, *5*, 41457-67. DOI
98. He, H.; Lian, J.; Chen, C.; Xiong, Q.; Zhang, M. Super hydrophilic carbon fiber film for freestanding and flexible cathodes of zinc-ion hybrid supercapacitors. *Chem. Eng. J.* **2021**, *421*, 129786. DOI
99. Li, Y.; Yang, W.; Yang, W.; et al. Towards high-energy and anti-self-discharge Zn-Ion hybrid supercapacitors with new understanding of the electrochemistry. *Nano-Micro. Lett.* **2021**, *13*, 1-16. DOI PubMed PMC

100. Chen, S.; Ma, L.; Zhang, K.; Kamruzzaman, M.; Zhi, C.; Zapien, J. A. A flexible solid-state zinc ion hybrid supercapacitor based on co-polymer derived hollow carbon spheres. *J. Mater. Chem. A.* **2019**, *7*, 7784-90. DOI
101. Zhou, H.; Liu, C.; Wu, J.; et al. Boosting the electrochemical performance through proton transfer for the Zn-ion hybrid supercapacitor with both ionic liquid and organic electrolytes. *J. Mater. Chem. A.* **2019**, *7*, 9708-15. DOI
102. Jin, T.; Li, H.; Zhu, K.; Wang, P. F.; Liu, P.; Jiao, L. Polyanion-type cathode materials for sodium-ion batteries. *Chem. Soc. Rev.* **2020**, *49*, 2342-77. DOI
103. Zeng, J.; Dong, L.; Sun, L.; et al. Printable zinc-ion hybrid micro-capacitors for flexible self-powered integrated units. *Nano-Micro. Lett.* **2020**, *13*, 19. DOI PubMed PMC
104. He, H.; Lian, J.; Chen, C.; Xiong, Q.; Li, C. C.; Zhang, M. Enabling multi-chemisorption sites on carbon nanofibers cathodes by an in-situ exfoliation strategy for high-performance Zn-ion hybrid capacitors. *Nano-Micro. Lett.* **2022**, *14*, 106. DOI
105. Zhang, W.; Yin, J.; Sun, M.; et al. Direct pyrolysis of supermolecules: an ultrahigh edge-nitrogen doping strategy of carbon anodes for potassium-ion batteries. *Adv. Mater.* **2020**, *32*, 2000732. DOI
106. Yuan, F.; Shi, C.; Li, Q.; et al. Unraveling the effect of intrinsic carbon defects on potassium storage performance. *Adv. Funct. Mater.* **2022**, *32*, 2208966. DOI
107. Zhang, Y.; Zhu, C.; Xiong, Y.; et al. Multi-channel hollow carbon nanofibers with graphene-like shell-structure and ultrahigh surface area for high-performance Zn-ion hybrid capacitors. *Small. Methods.* **2023**, *7*, 2300714. DOI
108. Hou, L.; Cui, X.; Guan, B.; et al. Synthesis of a monolayer fullerene network. *Nature* **2022**, *606*, 507-10. DOI
109. Wu, S.; Chen, Y.; Jiao, T.; et al. An aqueous Zn-ion hybrid supercapacitor with high energy density and ultrastability up to 80000 cycles. *Adv. Energy. Mater.* **2019**, *9*, 1902915. DOI
110. Sun, G.; Xiao, Y.; Lu, B.; et al. Hybrid energy storage device: combination of zinc-ion supercapacitor and zinc-air battery in mild electrolyte. *ACS. Appl. Mater. Interfaces.* **2020**, *12*, 7239-48. DOI
111. Liu, J.; Khanam, Z.; Ahmed, S.; Wang, T.; Wang, H.; Song, S. Flexible antifreeze Zn-ion hybrid supercapacitor based on gel electrolyte with graphene electrodes. *ACS. Appl. Mater. Interfaces.* **2021**, *13*, 16454-68. DOI
112. Wang, H.; Ye, W.; Yang, Y.; Zhong, Y.; Hu, Y. Zn-ion hybrid supercapacitors: achievements, challenges and future perspectives. *Nano. Energy.* **2021**, *85*, 105942. DOI
113. Poudel, M. B.; Balanay, M. P.; Lohani, P. C.; Sekar, K.; Yoo, D. J. Atomic engineering of 3D self-supported bifunctional oxygen electrodes for rechargeable zinc-air batteries and fuel cell applications. *Adv. Energy. Mater.* **2024**, *14*, 2400347. DOI
114. Jia, D.; Shen, Z.; Lv, Y.; et al. In situ electrochemical tuning of MIL-88B(V)@rGO into amorphous V_2O_5@rGO as cathode for high-performance aqueous zinc-ion battery. *Adv. Funct. Mater.* **2024**, *34*, 2308319. DOI
115. Wu, Y.; Yuan, W.; Wang, P.; et al. Conformal engineering of both electrodes toward high-performance flexible quasi-solid-state Zn-ion micro-supercapacitors. *Adv. Sci.* **2024**, *11*, 2308021. DOI
116. Yao, L.; Wu, Q.; Zhang, P.; et al. Scalable 2D hierarchical porous carbon nanosheets for flexible supercapacitors with ultrahigh energy density. *Adv. Mater.* **2018**, 30. DOI
117. Tian, W.; Gao, Q.; Tan, Y.; Li, Z. Unusual interconnected graphitized carbon nanosheets as the electrode of high-rate ionic liquid-based supercapacitor. *Carbon* **2017**, *119*, 287-95. DOI
118. Liu, S.; Zhou, J.; Song, H. 2D Zn-hexamine coordination frameworks and their derived N-rich porous carbon nanosheets for ultrafast sodium storage. *Adv. Energy. Mater.* **2018**, *8*, 1800569. DOI
119. Yu, J.; Yu, C.; Guo, W.; et al. Decoupling and correlating the ion transport by engineering 2D carbon nanosheets for enhanced charge storage. *Nano. Energy.* **2019**, *64*, 103921. DOI
120. Cao, Y.; Tang, X.; Liu, M.; et al. Thin-walled porous carbon tile-packed paper for high-rate Zn-ion capacitor cathode. *Chem. Eng. J.* **2022**, *431*, 133241. DOI
121. Zhang, H.; Chen, Z.; Zhang, Y.; et al. Boosting Zn-ion adsorption in cross-linked N/P co-incorporated porous carbon nanosheets for the zinc-ion hybrid capacitor. *J. Mater. Chem. A.* **2021**, *9*, 16565-74. DOI
122. Xu, Z.; Sun, Z.; Shan, J.; et al. O, N-codoped, self-activated, holey carbon sheets for low-cost and high-loading zinc-ion supercapacitors. *Adv. Funct. Mater.* **2024**, *34*, 2302818. DOI
123. Wang, H.; Chen, X.; Zhang, J.; et al. Unveiling the cooperative roles of pyrrolic-N and carboxyl groups in biomass-derived hierarchical porous carbon nanosheets for high energy-power Zn-ion hybrid supercapacitors. *Appl. Surf. Sci.* **2022**, *598*, 153819. DOI
124. Panmand, R. P.; Patil, P.; Sethi, Y.; et al. Unique perforated graphene derived from Bougainvillea flowers for high-power supercapacitors: a green approach. *Nanoscale* **2017**, *9*, 4801-9. DOI
125. Han, X.; Funk, M. R.; Shen, F.; et al. Scalable holey graphene synthesis and dense electrode fabrication toward high-performance ultracapacitors. *ACS. Nano.* **2014**, *8*, 8255-65. DOI
126. Liu, P.; Kong, F.; Tang, H.; et al. Hierarchically porous carbon nanosheets derived from bougainvillea petals with "pores-on-surface" structure for ultrahigh performance Zinc-ions hybrid capacitors. *Chem. Eng. J.* **2024**, *491*, 151944. DOI
127. Zhang, G.; Song, Y.; Zhang, H.; Xu, J.; Duan, H.; Liu, J. Radially aligned porous carbon nanotube arrays on carbon fibers: a hierarchical 3D carbon nanostructure for high-performance capacitive energy storage. *Adv. Funct. Mater.* **2016**, *26*, 3012-20. DOI
128. Pan, L.; Wang, Y.; Hu, H.; et al. 3D self-assembly synthesis of hierarchical porous carbon from petroleum asphalt for supercapacitors. *Carbon* **2018**, *134*, 345-53. DOI
129. Fleischmann, S.; Zhang, Y.; Wang, X.; et al. Continuous transition from double-layer to Faradaic charge storage in confined electrolytes. *Nat. Energy.* **2022**, *7*, 222-8. DOI

130. Chmiola, J.; Yushin, G.; Gogotsi, Y.; Portet, C.; Simon, P.; Taberna, P. L. Anomalous increase in carbon capacitance at pore sizes less than 1 nanometer. *Science* **2006**, *313*, 1760-3. DOI PubMed
131. Zeng, S.; Shi, X.; Zheng, D.; et al. Molten salt assisted synthesis of pitch derived carbon for Zn ion hybrid supercapacitors. *Mater. Res. Bull.* **2021**, *135*, 111134. DOI
132. Zhang, X.; Tian, X.; Song, Y.; Wu, J.; Yang, T.; Liu, Z. High-performance activated carbon cathodes from green cokes for Zn-ion hybrid supercapacitors. *Fuel* **2022**, *310*, 122485. DOI
133. Fleischmann, S.; Mitchell, J. B.; Wang, R.; et al. Pseudocapacitance: from fundamental understanding to high power energy storage materials. *Chem. Rev.* **2020**, *120*, 6738-82. DOI
134. Shi, X.; Xie, J.; Yang, F.; et al. Compacting Electric double layer enables carbon electrode with ultrahigh Zn ion storage capability. *Angew. Chem. Int. Ed.* **2022**, *61*, e202214773. DOI
135. Zhang, H.; Liu, Q.; Fang, Y.; et al. Boosting Zn-ion energy storage capability of hierarchically porous carbon by promoting chemical adsorption. *Adv. Mater.* **2019**, *31*, 1904948. DOI
136. Chen, H.; Lu, X.; Wang, H.; Sui, D.; Meng, F.; Qi, W. Controllable fabrication of nitrogen-doped porous nanocarbons for high-performance supercapacitors via supramolecular modulation strategy. *J. Energy. Chem.* **2020**, *49*, 348-57. DOI
137. Peng, X.; Zhang, L.; Chen, Z.; et al. Hierarchically porous carbon plates derived from wood as bifunctional ORR/OER electrodes. *Adv. Mater.* **2019**, *31*, 1900341. DOI
138. Deng, J.; Peng, Z.; Xiao, Z.; Song, S.; Dai, H.; Li, L. Porous doped carbons from anthracite for high-performance supercapacitors. *Appl. Sci.* **2020**, *10*, 1081. DOI
139. Li, H.; Su, P.; Liao, Q.; et al. Olive leaves-derived hierarchical porous carbon as cathode material for anti-self-discharge zinc-ion hybrid capacitor. *Small* **2023**, *19*, 2304172. DOI
140. Chen, G.; Chen, S.; Wu, X.; et al. Ammonium persulfate assisted synthesis of ant-nest-like hierarchical porous carbons derived from chitosan for high-performance supercapacitors and zinc-ion hybrid capacitors. *J. Mater. Chem. A.* **2024**, *12*, 11920-35. DOI
141. Xu, Y.; Sheng, K.; Li, C.; Shi, G. Self-assembled graphene hydrogel via a one-step hydrothermal process. *ACS. Nano.* **2010**, *4*, 4324-30. DOI
142. Cong, H. P.; Ren, X. C.; Wang, P.; Yu, S. H. Macroscopic multifunctional graphene-based hydrogels and aerogels by a metal ion induced self-assembly process. *ACS. Nano.* **2012**, *6*, 2693-703. DOI
143. Wu, Z. S.; Sun, Y.; Tan, Y. Z.; Yang, S.; Feng, X.; Müllen, K. Three-dimensional graphene-based macro- and mesoporous frameworks for high-performance electrochemical capacitive energy storage. *J. Am. Chem. Soc.* **2012**, *134*, 19532-5. DOI PubMed
144. Chen, Y.; Kone, I.; Gong, Y.; et al. Ultra-thin carbon nanosheets-assembled 3D hierarchically porous carbon for high performance zinc-air batteries. *Carbon* **2019**, *152*, 325-34. DOI
145. Largeot, C.; Portet, C.; Chmiola, J.; Taberna, P. L.; Gogotsi, Y.; Simon, P. Relation between the ion size and pore size for an electric double-layer capacitor. *J. Am. Chem. Soc.* **2008**, *130*, 2730-1. DOI PubMed
146. Xu, X.; Zhao, X.; Yang, Z.; et al. High-density three-dimensional graphene cathode with a tailored pore structure for high volumetric capacity zinc-ion storage. *Carbon* **2022**, *186*, 624-31. DOI
147. Zou, T.; Ding, H.; Qian, C.; et al. Three-dimensional graphene-wrapped $CoSe_2$ nanowires for high-performance asymmetric supercapacitors. *ACS. Appl. Nano. Mater.* **2023**, *6*, 10466-76. DOI